energies

MDPI

Review

Electrochemically Structured Copper Current Collectors for Application in Energy Conversion and Storage: A Review

Mario Kurniawan and Svetlozar Ivanov *

Electrochemistry and Electroplating Group, Department of Electrical Engineering and Information Technology, Technische Universität Ilmenau, Gustav-Kirchhoff-Straße 6, 98693 Ilmenau, Germany; mario.kurniawan@tu-ilmenau.de

* Correspondence: svetlozar-dimitrov.ivanov@tu-ilmenau.de

Abstract: Copper current collectors (Cu CCs) impact the production technology and performance of many electrochemical devices by their unique properties and reliable operation. The efficiency of the related processes and the operation of the electrochemical devices could be significantly improved by optimization of the Cu CCs. Metallic Cu plays an important role in electrochemical energy storage and electrocatalysis, primarily as a conducting substrate on which the chemical processes take place. Li nucleation and growth can be influenced by the current collector by modulating the local current density and Li ion transport. For example, the commonly used planar Cu CC does not perform satisfactorily; therefore, a high number of different modifications of Cu CCs have been proposed and reported in the literature for minimizing the local current density, hindering Li dendrite formation, and improving the Coulombic efficiency. Here, we provide an updated critical overview of the basic strategies of 3D Cu CC structuring, methodologies for analyzing these structures, and approaches for effective control over their most relevant properties. These methods are described in the context of their practical usefulness and applicability in an effort to aid in their easy implementation by research groups and private companies with established traditions in electrochemistry and plating technology. Furthermore, the current overview could be helpful for specialists with experience in associated fields of knowledge such as materials engineering and surface finishing, where electrochemical methods are frequently applied. Motivated by the importance of the final application of Cu CCs in energy storage devices, this review additionally discusses the relationship between CC properties and the functional parameters of the already-implemented electrodes.

Keywords: copper; current collector; Li ion battery; energy storage; 3D structuring; AAO template; dynamic hydrogen bubble template

Citation: Kurniawan, M.; Ivanov, S. Electrochemically Structured Copper Current Collectors for Application in Energy Conversion and Storage: A Review. *Energies* **2023**, *16*, 4933. https://doi.org/10.3390/en16134933

Academic Editor: Huang Zhang

Received: 10 June 2023
Revised: 19 June 2023
Accepted: 21 June 2023
Published: 25 June 2023

1. Introduction

Owing to its good processability, high availability, relatively low cost, chemical inertness with respect to Li, and favorable electrical properties, metallic Cu plays an important role in modern energy technology. Currently, Cu current collectors (CCs) are broadly implemented in rechargeable batteries, e.g., Li ion batteries (LIBs) (Figure 1a), ultracapacitors, and electrocatalysis [1,2]. Following the invention of the LIB in the late 1970s, one of the most frequent Cu CC applications in energy conversion and storage has involved a standard Cu foil on which active battery materials are typically coated to enable normal operation of the LIB anode (Figure 1a). Nevertheless, the need for a prompt energy transition imposed by the contemporary environmental and political issues has resulted in the development of diverse technological improvements, including significant advances in the fabrication of more efficient and practical Cu CCs.

The CCs in rechargeable batteries are chemically inactive materials in their local environment; however, their properties can greatly influence battery operation and parameters [1]. For example, the relative weight of the CCs in LIBs is currently approaching

15%, displaying a high impact on the final energy density of the battery [1] (Figure 1b) and good prospects for improvement by adjusting the CC thickness and rationalizing the cell design [1]. A logical way to realize these expectations is the structuring of the Cu CCs, i.e., formation of 3D CCs, which has been associated with various functional advantages since their initial development in the early 2000s (Figure 1c) [1–3].

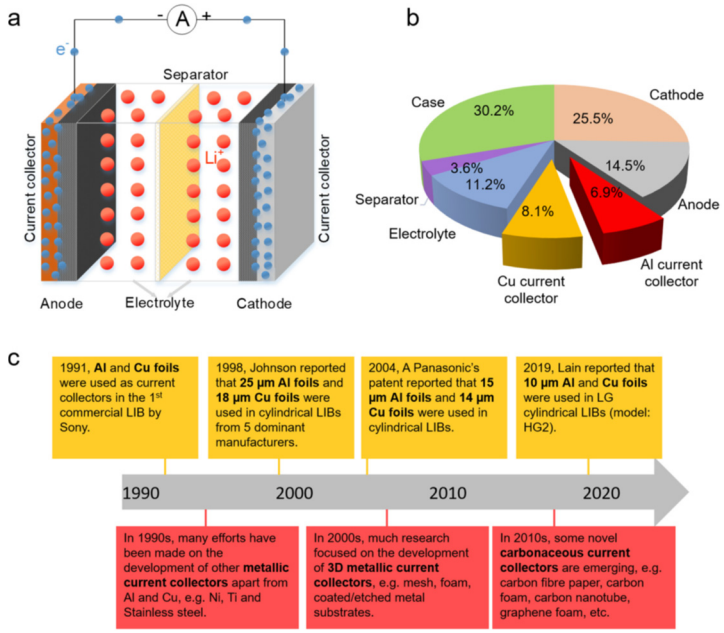

Figure 1. (**a**) Schematic diagram of a typical Li ion battery, (**b**) weight percentages of the main components in an LIB, (**c**) historical timeline of the development of current collectors for LIBs in industry (yellow) and academia (red) [1] (with permission from Elsevier).

The high active surface area of CCs with a 3D geometry is provided by the internal pore structure, where lightweight design has been well realized. This approach helps to reduce the local current density and polarization of the anode, and in this way, the kinetics of the negative electrode reaction can be improved [4–7]. Furthermore, compared to flat CCs, the pore network of 3D CCs can successfully accommodate the expansion of many active materials during insertion of Li or other guest ions. Appropriate examples of this effect are related to deposited materials such as Si, Sn, transition metal oxides (TMOs), etc., known to have Li insertion-related mechanical instability [1,2]. In addition, 3D structuring of CCs has a positive impact on the ionic transport in the electrode by shortening the diffusion length of the Li ions [8]. The improvement of this parameter is important for accelerating the reaction kinetics under diffusion limitations, where the ionic transport plays a rate-limiting role.

There are different methods for the formation of 3D-structured Cu CCs, which are generally classified into template-assisted and template-free approaches [9,10]. Depending on process conditions, differences in length scale and the form of the 3D Cu structures can be obtained [1,2,6]. However, from a practical point of view the methods with minimal energy consumption, reduced number of technological steps, and utilization of non-toxic reagents are more favorable. In many cases, for example, technological stages involving high-temperature thermal treatments, expensive deposition equipment, e.g., Chemical Vapor Deposition (CVD), Physical Vapor Deposition (PVD), Atomic Layer Deposition (ALD), and toxic chemicals, e.g., HF-based etching baths are utilized. Therefore, the application of practical methods that allow for effective optimization of the Cu nano- and microstructure are necessary to realize improvements in cost, environmental impact, and technical usefulness across a broad spectrum of applications. In view of this, electrochemical methods enable much simpler and low-cost fabrication processing [11]. At the same time,

electrochemical techniques such as electroplating and anodization are versatile options owing to the possibility of adjusting the properties of the obtained or modified materials and providing better freedom of choice with regard to the form and nature of the used substrates. In this context, a number of 3D Cu formation methodologies are based on or involve electrochemical methods, which are considered technologically more effective and much simpler in comparison with their non-electrochemical alternatives [11].

An important step that belongs to the implementation of 3D Cu CC technology is the characterization of the structured Cu CC properties. Here, the list of practically relevant parameters comprises the active surface area, porosity and tortuosity, electrical properties, mechanical characteristics, stability, and interfacial properties [2]. In order to realize a complete characterization of the Cu CC properties, a broad variety of instrumental methods have to be employed; however, these require extra investment costs and outsourcing, which is usually challenging for small and midsize companies and small research labs. Therefore, fast, simple, and economical characterization strategies, closely related to the final goal of CCs implementation have always been preferred by both industry and researchers in applied fields.

This review paper introduces readers to the basic approaches of structured 3D Cu CC fabrication involving electrochemical processing. The main factors which influence electrochemical Cu CC formation are critically discussed and exemplified with an appropriately updated literature overview. As the effective characterization of 3D structured Cu CCs may be one of the obstacles to the development of advanced high-energy storage technologies, a separate section of this review is devoted to the presentation of specific electrochemical methods representing simple and low-cost options for Cu CC analysis. These methods are described in the context of their practical usefulness and applicability, with the aim of enabling easy implementation by research groups and private companies with established traditions in electrochemistry and plating technology. Furthermore, the current overview could be helpful to specialists with experience in associated fields of knowledge such as materials engineering and surface finishing, where electrochemical methods are frequently applied. Motivated by the importance of the final application of the Cu CCs in energy storage devices, this paper additionally discusses the interrelations between CC properties and the functional parameters of the already-implemented electrodes.

2. Electrochemical Methods for 3D Cu CC Formation

The main electrochemistry-based techniques used for the formation of various Cu CC 3D morphologies (e.g., nanowires, nanopillars, nano- and microporous layers, foam structures, etc.) are presented in this section. These methods are categorized according to their mechanism of application into (1) template-assisted and (2) template-free. Common to both these approaches is that their methodology involves one or more electrochemical steps. The impact of the specific working strategies and experimental conditions on the morphology and properties of the resulting Cu structures are discussed individually below.

2.1. Template-Assisted Methods

Templating is one of the key methodologies for the controlled fabrication of micro- and nanostructured materials. This approach relies on formation/synthesis or assembly of a pre-existing pattern (template) with desired nanoscale features (first step). The role of this pattern is to direct the deposition of nanomaterials into forms that are otherwise difficult or impossible to obtain (second step). Finally, to obtain the desired structured Cu array, the applied template has to be removed (third step). In the following subsections, template-assisted approaches for Cu deposition relying on different types of template nature and formation are presented.

2.1.1. AAO Templates

An anodic aluminum oxide (AAO) template is a self-organizing porous anodic layer of Al_2O_3 that typically has a honeycomb-like structure of pores aligned in parallel to forming

density arrays with a high number of pores. Among all templates, AAO layers are the most widely applied for nanowire growth (Figure 2). When using AAO templates, the nanowire diameter can be precisely determined by the AAO pore size [12]. The pore diameter can be adjusted in the range of five to several hundred nm, and the AAO thickness, which determines the nanowire length, can be controlled from a few tens of nanometers to a few hundred micrometers. Porous AAO templates are formed electrochemically by anodization of Al, typically in acid electrolytes, as reported by Masuda and Fukuda [13] and numerous later researchers [14]. Owing to their ordered uniform nanopores, AAO templates have been widely used in nanotechnology for the deposition of metallic and semiconductor nanowire arrays [14,15].

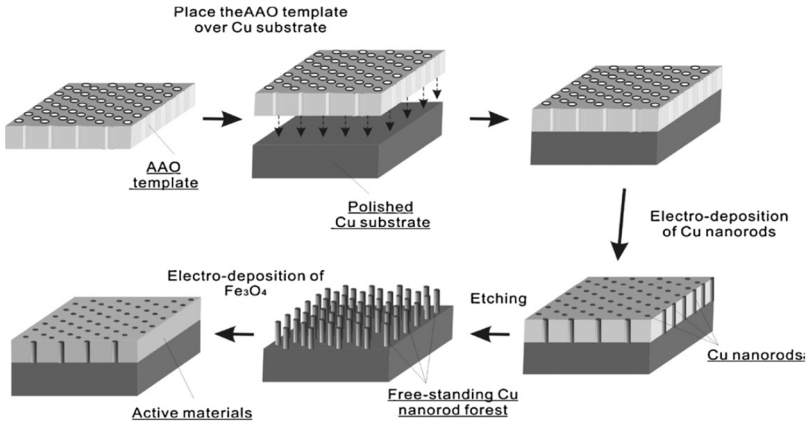

Figure 2. Schematic of free-standing Cu nanorod fabrication [15] (with permission from Elsevier).

The first reports on the electrochemical deposition of Cu in AAOs date back to the early 2000s [16], when the application of AAO-grown Cu nanowires as field emitters was first demonstrated [16]. The early demonstration of this technique was followed by many studies of AAO-templated Cu CC electrodeposition, mainly for electronics [17], electrocatalytic purposes [18], and energy storage applications [15].

AAO nanoporous templates with different pore diameters and interpore distances can be easily grown by potentiostatic anodization of aluminum carried out in acidic electrolytes. In particular, electrolyte solutions based on sulfuric acid, [19], oxalic acid [13,20,21], or phosphoric acid [22] can be applied. The geometry of the obtained AAO membranes strongly depends on electrochemical conditions, i.e., on parameters such as anodization voltage, electrolyte composition, and anodization time [23]. Generally, the AAO pore diameter and the interpore distance depend linearly on the applied potential/voltage. The influence of the experimental parameters (i.e., anodization potential, pH, electrolyte concentration, anodizing time, and pore widening time) on AAO pore diameter is schematically presented in Figure 3. In order to design an AAO template with specific pore dimensions, all factors influencing the pore formation process have to be taken into account [23].

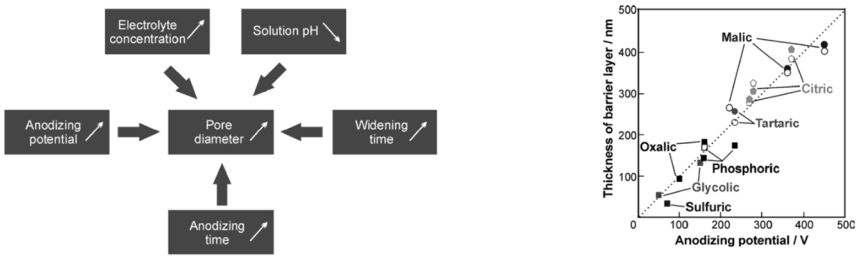

Figure 3. Parameters that influence AAO pore diameter, which are indicated by arrows (**left**) and thickness of the barrier layer as a function of the anodizing potential for AAO layers grown in different electrolytes (**right**) [23] (with permission from Wiley).

Barrier layer thickness is one of the most important AAO parameters (Figure 4, left); in order to realize nanowire electrodeposition, either its thickness has to be reduced or the entire barrier layer has to be removed. The AAO wall thickness and barrier layer thickness can be modified during the post-treatment process, which usually involves a chemical etching step [23].

The strategies for the fabrication of Cu nanowire arrays can be generally categorized into three main groups [22]. In the first approach, a thin layer of conductive metal is deposited on through-hole AAO membranes, followed by galvanostatic Cu electrodeposition [24]. However, to obtain a nanoporous AAO layer with open-ended channels, the remaining Al metal has to be removed, and in certain cases an extrapore widening step is necessary. The second method consists of alternating-current (AC) Cu electrodeposition inside the AAO pores, and does not require any additional processing after Al anodization [25,26]. This technique allows for the growth of large quantities of Cu nanowires [26]. The third interesting approach applies a through-hole AAO template as a direct mask for the electrodeposition of Cu nanowire arrays [15,27]. The main advantage of this method is its simple manufacturing process. Nevertheless, this strategy relies on strong adhesion of the AAO template to the surface of the Cu substrate [27].

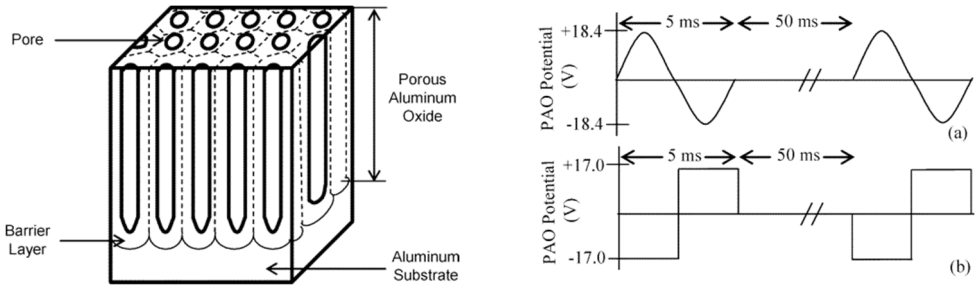

Figure 4. Schematic diagram of porous aluminum oxide template (**left**). Schematics of two of the wave shapes and pulse polarities employed in this work (**right**): a pulsed sine wave with oxidative/reductive pulse polarity (**a**), and a pulsed square wave with reductive/oxidative pulse polarity (**b**) [25] (with permission from the American Chemical Society).

In nearly all scientific works in the field, $CuSO_4$ is the Cu source of the electrolyte composition and Cu electrodeposition in acidic and alkaline electrolytes is possible. Acid electrolytes are frequently used for this purpose due to their high efficiency and the higher current density that can be applied when using these solutions. Their main drawback is their low throwing power and the pronounced corrosion caused by the more chemically active metals in these media (e.g., Zn, Fe, Sn, etc.). Alkaline copper electrolytes display higher throwing power than acidic ones; they are less corrosive, and as such are especially important for the industrial plating of steel and other non-inert substrates. Nevertheless, the high toxicity and corresponding environmental issues of the most frequently used alkaline cyanide electrolytes motivate the development of less toxic alternative solutions based on other complexing agents such as sorbitol, glycine, glycerol, glutamate, and pyrophosphate [28]. Copper electrodeposition in AAOs is performed mainly in two electrode cells using different cell geometries. Furthermore, a variety of electrochemical procedures are used for deposition of Cu in the AAO nanopores, including DC galvanostatic and potentiostatic deposition and different AC (pulse) techniques (Figure 4, right). The specific cell and electrode geometries and the application of different substrates, procedures, and electrolytes make comparative analysis of the results reported in the literature difficult. Therefore, to achieve the desired properties of Cu deposits reported in individual research contributions, the experimental conditions have to be strictly reproduced. Information about electrolyte composition, electrochemical deposition parameters, cell configuration, substrates, and Cu array dimensions is summarized in Table 1.

Table 1. Copper deposition conditions and wire diameter summarized from selected works for AAO template technique.

Electrolyte	Electrochemical Parameters	Cell Configuration/ Substrate	Cu Wire Diameter /nm	Ref.
0.5 M $CuSO_4$ and 0.5 M H_2SO_4	DC galvanostatic j = 2 mA cm^{-2}	three-electrode	80	[22]
A: (200 g L^{-1} $CuSO_4 \cdot 5H_2O$, 90 g L^{-1} H_2SO_4) B: (60 g L^{-1} $CuSO_4 \cdot 5H_2O$, 180 g $L^{-1}H_2SO_4$, 70 mg L^{-1}HCl). C: (100 g L^{-1} $CuSO_4 \cdot 5H_2O$, 10 g L^{-1} $(NH_4)_2SO_4$, 40 mL L^{-1} diethylenetriamine (DETA))	DC potentiostatic E = 0.1–1 V	two-electrode Al vs. Cu	200	[29]
100 g L^{-1} $CuSO_4 \cdot 5H_2O$, 20 g L^{-1} $(NH_4)_2SO_4$, and 80 mL L^{-1} DETA	DC potentiostatic E = 1.2 V	two-electrode 2 Cu disks	200	[15]
100 g L^{-1} $CuSO_4$ $5H_2O$, 20 g L^{-1} $(NH_4)_2SO_4$, 80 mL L^{-1} DETA	two-step pulse cathodic current profile: −0.002 A, 0.25 s, −0.03 A, 0.05 s, 20,000 cycles	two-electrode Ni vs. Cu	200	[30]
100 g L^{-1} $CuSO_4 \cdot 5H_2O$, 20 g L^{-1} $(NH_4)_2SO_4$, 80 mL L^{-1}DETA,	1st step: 250 ms pulse E = −1.7 V vs. Ag/AgCl, 2nd step: 250 and 50 ms, pulses j = −6 and j = −90 mA cm^{-2}, respectively	three-electrode Cu vs. Cu	340	[31]
100 g L^{-1} $CuSO_4 \cdot 5H_2O$, 20 g L^{-1} $(NH_4)_2SO_4$, 80 mL L^{-1} DETA,	DC, galvanostatic j = −2 mAcm^{-2}, 250 ms. For the next 50 ms, j = −30 mA cm^{-2}	two-electrode Cu-Cu	200	[27]
0.5 M $CuSO_4$, 0.5 M H_2SO_4	DC galvanostatic j = 5 mA cm^{-2} t = 60 min	three-electrode Pt pseudo-reference and counter electrodes	60–105	[32]
0.50 M $CuSO_4$, 0.285 M H_3BO_3	continuous 200 Hz sine wave at 10 V_{rms} for 10 min	anodized Al cathode and 2 Cu plates anodes	16	[28]
238 g L^{-1} $CuSO_4 \cdot 5H_2O$ and 2 g/L H_2SO_4	DC, potentiostatic the applied voltage was 2 V.	two-electrode	50–80	[33]
250 g L^{-1} $CuSO_4 \cdot 5H_2O$, 45 g L^{-1} H_3BO_3	identical duty cycle consisting of 5 ms for the working regime (−8.5 V vs. Ag/AgCl) and 95 ms of resting regime (0 V vs. Ag/AgCl) at various negative voltages	three-electrode, Ag/AgCl reference, graphite counter electrode.	27–86	[34]
0.50 M $CuSO_4$, 0.57 M H_3BO_3	wave and pulse polarity 200 Hz (5-ms duration) single pulses triggered at 20 Hz (50-ms intervals), sine wave voltage of 13 Vrms (18.4 Vpeak), square wave voltage of 17 Vpeak.	two-electrode Pt counter	20–35	[25]
0.4 M $CuSO_4$, 10% H_2SO_4 (pH = 2.5)	DC, galvanostatic j = 0.001 A	two-electrode Cu-Al	40–80	[35]
0.3 M $CuSO_4$ 0.1 M H_3BO_3	DC, potentiostatic −0.3 V vs. Ag | AgCl for 30 min	three-electrode	35	[36]

2.1.2. Track-Etched Polymer Membrane Templates

Track Etched Membranes (TFM) are precisely fabricated polymer layers, with multiple applications in life sciences, engineering, and nanotechnology. These functional materials can be produced with a pre-defined pore diameter, with each pore being able to form a single channel throughout the entire membrane thickness. The TFM can have a film thickness from 6 to 50 µm for different polymer materials, including polycarbonate (PC), polyethylene terephthalate (PET), polyvinylidene difluoride (PVDF), polypropylene (PP), and polyimide (PI). Among all polymer types, PC and PET are the most studied materials for application of TEM in nanotechnology. In particular, PC dominates research work in the field of metallic nanowire deposition. The process of TEM fabrication involves two steps, ion tracking and chemical etching [37]; the fabrication technique consists of the formation of continuous trails in the material by exposure to radiation (first step) and the formation of fine holes by preferentially dissolving the damaged trails in an appropriate etching bath (second step). These holes can be chemically enlarged by regulating the etching time until the necessary size is achieved [37,38]. There are two radiation-based methods for the formation of tracks on polymer films: (1) bombardment with heavy particles (e.g., alfa radiation), and (2) use of high-energy ion beams from accelerators (e.g., GSI, Darmstadt, Germany, and GANIL, Caen, France) [38]. Etching of the polymer membrane is easily achieved in alkaline solutions such as KOH or NaOH. This allows the pore size to be enlarged and chemical moieties to be added to the inner pore surface. PC and PET membranes have similar properties; however, PC is more soluble in organic solvents and more suitable for producing membranes with cylindrical nanopores, as the pore size is very homogeneous and smooth [38].

Similar to AAO, PC membranes with relatively narrow pore diameters (close to 10 nm) are commercially available; furthermore, they can be used as a template to grow metal nanowire arrays. Nevertheless, as discussed by Motoyama et al. [39], the geometrical periodicity of nanowire arrays is low compared to that of AAOs due to random hole formation during PC irradiation with heavy ion particles. Furthermore, the same authors observed the nonuniformity of nanowires along the length direction (Figure 5a), which has been attributed to the original irregular shape of the nanopore wall in PC membranes after track-etching with heavy ions. In this context, a broader pore size distribution was investigated earlier by Chlebny et al. [40] (Figure 5b). They concluded that electrochemical nanowire formation using such a template can be applied in fields such as energy conversion and storage where highly ordered arrays are not required [39].

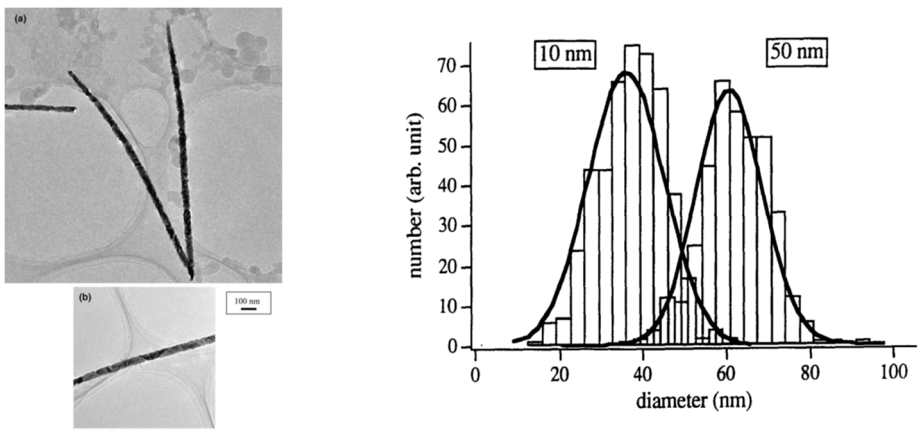

Figure 5. TEM imaging of Cu nanowires (**a**) and Ni nanowire (**b**) deposited by means of a PS template, demonstrating the irregular wire diameter (**left**) and diameter distribution of nanopores in PS membranes with nominal pore sizes of 10 and 50 nm (**right**) [38,39] (with permission from Elsevier).

The electrochemical conditions and morphological properties of the PC membrane templates, and corresponding Cu nanostructures are summarized in Table 2.

Table 2. Electrochemical deposition conditions and wire diameter for Cu nanowires grown using PC membrane template.

Electrolyte	Electrochemical Parameters	Cell Configuration/ Substrate	Cu Wire Diameter/ Template	Ref.
0.2 M $CuSO_4$ 0.4 M H_3BO_3	DC potentiostatic E = −1 V	Three-electrode Au sputtered PC template (WE), SCE reference, Pt-counter	Cu nanorods; TEM (Whatman) PC membranes d = 50 nm	[41]
220 g/L Cu_2SO_4 $5H_2O$ 32 g/L H_2SO_4	DC potentiostatic E = 200 mV	Two-electrode Cu anode, Au cathode	30 µm-thick PC foils (Makrofol-N, Bayer Leverkusen) d = 25 nm	[42]
2.5 N (200 g/L) $CuSO_4 \cdot 5H_2O$ pH 3.14.	DC galvanostatic j = 65−0.6 mA/cm^2	Two-electrode Cu anode	Nuclepore PC membranes d_{pore} = 800 nm, 11 µm thickness	[43]
200 g $CuSO_4$ $5H_2O$ H_2SO_4 (10–12 drops) pH 0.9.	DC potentiostatic E = 0.8 V (current 0.0137–0.0140 A)	Two-electrode Cu anode	10 mm PC (Makrofol KG) foil d_{pore} = 10 nm	[44]
0.60 M $CuSO_4$, 5×10^{-3} M H_2SO_4 (pH 1.7)	DC potentiostatic E = −0.4 V vs. Cu quasi−reference	Three-electrode	PC membrane d = 50, 80 nm (Nomura Micro Science Co. Ltd., Okata, Japan), (Toyo Roshi Kaisha Ltd., Tokyo, Japan). d = 100, and 200 nm	[45]
0.5 M $CuSO_4 \cdot 5H_2O$ 0.01 M H_2SO_4.	DC potentiostatic Overpotential η = −150 mV	Three-electrode Au sputtered onto one side of the PC and reinforced with electrodeposited Cu, Ag/AgCl reference	PC Nuclepore, Whatman, d_{pore} = 100 nm	[46]
590 mg/L $CuSO_4.5H_2O$ 30 g/L H_3BO_3.	DC, potentiostatic E = 0.4 V,	Three-electrode Pt counter, Ag/AgCl reference, Au or ITO working	PC spin-coated, irradiated in the accelerator of the Centre de recherches du Cyclotron at Louvain-la-Neuve d_{pore} = 15–100 nm	[47]
75 g L^{-1} $CuSO_4 \cdot 5H_2O$ varied H_2SO_4 concentrations	DC potentiostatic E = 90–500 mV	Two-electrode	PC (Makrofol N, Bayer Leverkusen) thickness 30 µm d_{wire} = 75 nm	[48]
0.55 M H_2SO_4, 0.88 M $CuSO_4$	DC potentiostatic, E = −0.4 V to −0.25 V Vs. Cu ref	Three-electrode	(PC) membranes purchased from SPI-pore, d_{wire} = 400–450 nm	[49]

2.1.3. Particle Templates

Another template approach is based on the initial assembly of spherical particles on the substrate surface, followed by Cu electrodeposition and subsequent removal of the initially assembled template structure. This so-called colloid assembling technique has attracted many research groups owing to its easy and low-cost formation of 3D macroporous layers [50,51]. Liquid–air interfaces have been used for the self-assembly of colloidal particles with a diameter of several hundred nanometres, finally resulting in the formation of regularly ordered large particle arrays. When performing template self-assembly, PS or SiO_2 sub-micron-sized spheres are typically used. During self-assembly, capillary forces

trigger the formation of a dry colloidal fcc crystal resulting in a structure called artificial opal, and the material deposited in the interstitial spaces is named inverse opal [50].

Following this approach, porous metallic structures can be formed through electrodeposition in self-assembled PS or other particles. This technique was initially used for gold [52], and later microporous copper material was deposited using the same method [53,54]. Following electrodeposition, the original opal material can be removed. For example, etching of silica opal is performed by immersion in a 5% solution of HF [55] and opal formed of PS can be removed by combustion at 450 °C or by dissolving the PS template in organic solvents, e.g., toluene [54].

The deposition of high-quality 3D porous copper and other porous metal films using this method depends critically on factors that control the permeability of the electrolyte solution in the nanochannels of the PS template. Ding et al. concluded that the permeability can be substantially increased by surface modification of the PS template, which has the aim of enhancing the hydrophilicity of the PS particles [53,54]. Such an effect was realized by modification of the PS surface with SDS in [53] (Figure 6).

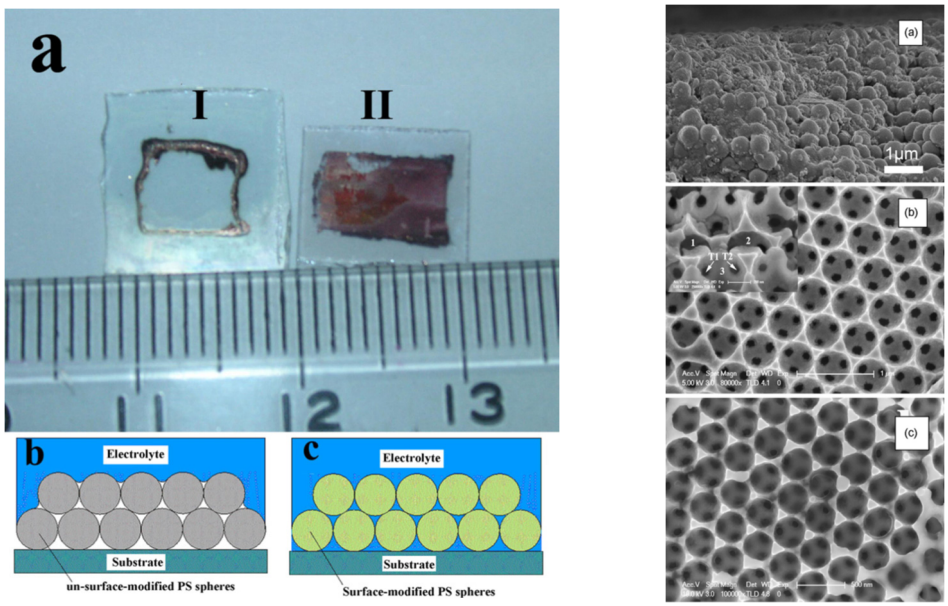

Figure 6. A photograph (**left**) of electrodeposited samples, showing the contrast in permeability of the electrolyte in the voids enclosed by the PSs: (**a**) the templates used for samples I and II were respectively unmodified and modified with SDS; (**b**,**c**) schemes showing the permeability of the electrolyte with and without surface-modification, respectively. SEM images (**right**) of 3D macroporous copper films: (**a**) the section of copper film before removal of the colloid template, (**b**,**c**) the pore sizes of 490 nm and 345 nm, respectively [54] (with permission from Elsevier).

Another useful approach for mitigation of permeability issues when depositing PS opal is choosing electrolytes with better wetting properties. In this context, Tsai et al. [56] utilized ionic liquid (IL) electrolytes for the electrodeposition of macroporous silver using PS opal templates. The authors observed that their ILs ([BMP][TFSI] and [BMP][DCA]) displayed improved wetting on the hydrophobic PS templates compared to the aqueous electrolytes. This approach has been demonstrated for copper electrodeposition as well. Zein El Abedin et al. [57] reported on the electrodeposition of highly ordered macroporous copper films in 1-butyl-3-methylimidazolium dicyanamide ([BMIm][DCA]) using PS opal templates. PS colloidal spheres were assembled onto gold and indium tin oxide (ITO) substrates, displaying an ordered hexagonal structure. Afterwards, the interstitial spaces of the PS opal arrays were filled with copper by electrodeposition. Well-ordered macroporous copper films have been obtained after the chemical dissolution of the PS template. Further-

more, highly ordered 2Dand 3D macroporous Cu films with interconnected pore structures can be fabricated by varying the experimental conditions.

Practically useful information about the experimental electrochemical conditions and morphology of structured Cu obtained using this method is summarized in Table 3.

Table 3. Electrochemical deposition conditions and morphology for Cu deposits grown using particle assembly templates.

Electrolyte	Electrochemical Parameters	Cell Configuration/ Substrate/ Template	Morphology	Ref.
60 g L^{-1} $Cu_2P_2O_7$, 280 g L^{-1} $K_4P_2O_7$ $3H_2O$ 20 g L^{-1} $(NH_4)_2HC_6H_5O_7$	DC galvanostatic I = 3 mA, t = 300 s	PS spheres ITO-Pt-SCE;	Porous ordered d = 486 nm;	[53,54]
0.2 M $CuCl_2$ [BMIm]DCA	DC potentiostatic E = − 0.15 V for 6 min E = − 0.2 V for 10 min E = − 0.6 V for 20 min.	PS spheres (Duke Scientific, Fremont, CA, USA) Au-sputtered and ITO glass Cu-counter Cu-reference	Porous ordered d = 600 nm	[57]
0.1 M $CuSO_4$, 5 mL L^{-1} PEG400 MW 1×10^{-6} M KCl	DC potentiostatic E= −0.1 V vs. Ag | AgCl	PS latex spheres (Duke Scientific Corporation,) three-electrode Cu working, SS counter, Ag | AgCl reference	Porous Ordered d = 700 nm	[58]
commercial acidic Cu-plating solution containing $CuSO_4$	DC galvanostatic j = 10 mA cm^{-2} t = 3, 6, 9, and 12 min	PS template synthesized by electrophoretic deposition (EPD)	Porous Ordered d = 600 nm	[59]
0.6 M $CuSO_4$ 5 mM H_2SO_4	DC potentiostatic 40 min	PS spheres three-electrode	Microporous ordered d = 5 µm	[60]
100 g L^{-1},$CuSO_4 \cdot 5H_2O$ 20 g L^{-1} $(NH_4)_2SO_4$ 40 mL L^{-1} (DETA)	DC galvanostatic j = −3 mA cm^{-2} 5 min	Synthesized SiO_2 spheres Spin coated	Porous ordered d = 340 nm	[61]
9.0 mM $CuSO_4$, 5.0 mM H_2SO_4 pH 1.35	DC potentiostatic E= − 1.0–1.2 V t = 1200–3600 s	PS spheres Three-electrode Cu anode, PS-coated FTO glass cathode, SCE reference	Porous Ordered d = 300–500 nm	[62]
1.0 g $CuSO_4 \cdot 5H_2O$ in 5 mL of Millipore water 2.5 g DL-lactic acid pH 9.	DC potentiostatic E = −0.7 V–−0.3 V vs. Ag/AgCl.	PS (Micro-particles GmbH). three-electrode PS-coated substrate working, Pt counter, Ag/AgCl reference	Porous Ordered d = 248 nm	[63]

2.1.4. Dynamic Hydrogen Bubble Templates

As previously discussed, depending on the experimental conditions electrodeposition can lead to the formation of nanostructures of various geometric forms and dimensions. Dynamic Hydrogen Bubble Technique (DHBT) is a special type of electrodeposition technique that is particularly useful for the formation of 3D interconnected metallic structures (often called metallic foams). DHBT involves two parallel redox processes, namely, elec-

trodeposition and hydrogen evolution reaction (HER), where the hydrogen bubbles act as a dynamic template for the growth of the porous material. The DHBT technique has a number of important practical advantages, including (1) simple growth of porous material without the assistance of a solid template, (2) formation of micron-size layers consisting of nanostructured pore walls with high surface area, (3) an increased number of active sites at the pore walls, which help to accelerate chemical processes and allow easy modification, and (4) high mechanical stability [2].

The DHBT approach has been used for the fabrication of micro- and nanostructured foams across a broad spectrum of single elements, including copper. Among the high number of examples for DHBT-grown metallic foams, copper structures are the most frequently applied as electrode substrates in energy technologies. Owing to their lower hydrogen reduction overpotential, Cu foams can easily be formed and precisely tuned by adjusting DHBT parameters such as current density, deposition time, electrolyte composition, temperature, and substrate morphology [2].

Both the rate of Cu dendrite growth and the HER are greatly influenced by the applied current density and the corresponding overpotential. Here, the hydrogen bubble nucleation rate and its lifetime on the electrode play an important role. For example, at a lower current density a low number of irregularly distributed H_2 bubbles are generated on the substrate. This results in porous Cu with an irregular morphology. On the other hand, increased current density leads to HER acceleration, and consequently to improved pore regularity and decreased pore size [64]. The effect of current density on Cu deposit morphology is shown in Figure 7.

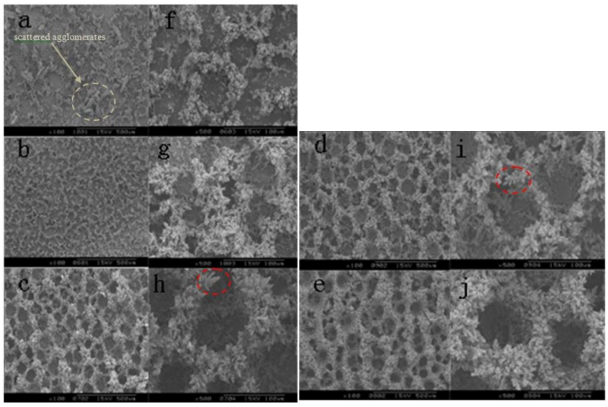

Figure 7. SEM images of porous copper films electrodeposited at different current densities: (**a**)/(**f**) 0.5 A·cm^{-2}, (**b**)/(**g**) 1 A·cm^{-2}, (**c**)/(**h**) 1.5 A·cm^{-2}, (**d**)/(**i**) 2 A·cm^{-2}, (**e**)/(**j**) 2.5 A·cm^{-2} [64] (open access).

Deposition time is another important factor that affects Cu pore morphology. It has been shown that the prolongation of deposition time at a constant current density results in enlarged pore diameter. This effect can be explained by the fact that the generated H_2 bubbles participate in physical processes such as collisions, deformation, coalescence, etc., each of which depends on the deposition time and influence the pore geometry [2].

The porous Cu morphology can be greatly influenced by temperature. It has been observed that increasing the electrolyte temperature leads to more intensive hydrogen evolution, resulting in a larger bubble template and an increase in the interstitial distance between the bubbles. Consequently, the pore size of the electrodeposited porous Cu foam increases, although electrolyte temperatures beyond 40 °C have a negative effect on grain size refinement and dendrite stability [64].

Adjusting the electrolyte composition is a useful tool for tuning the morphological properties of DHBT-synthesized Cu foams. Control over branching during Cu electrodeposition has been observed [65,66]; in particular, a reduction in branching has been found after addition of sulphates, chlorides, and bromides. Shin et al. [67] demonstrated that the pore size and wall structure of Cu foams can be changed by varying the electrolyte

composition. This effect is presented in Figure 8. The same authors observed that the addition of bubble stabilizer (e.g., acetic acid) suppresses the coalescence of H_2 bubbles, resulting in a lowering of their hydrophobic properties and a consequent reduction in pore size. Additionally, they found that the addition of chloride ions to the electrolyte leads to a decrease in branch size in the Cu foam walls as a result of the catalytic effect of chloride. In particular, it was observed that the pore size at the surface was reduced from 50 µm to about 25 µm when 0.1 M acetic acid was added to the electrolyte. A similar effect was achieved after the addition of cetyltrimethylammonium bromide (CTAB) [68]. Additionally, the branches formed on the pore walls were significantly reduced in size after the addition of HCl [67].

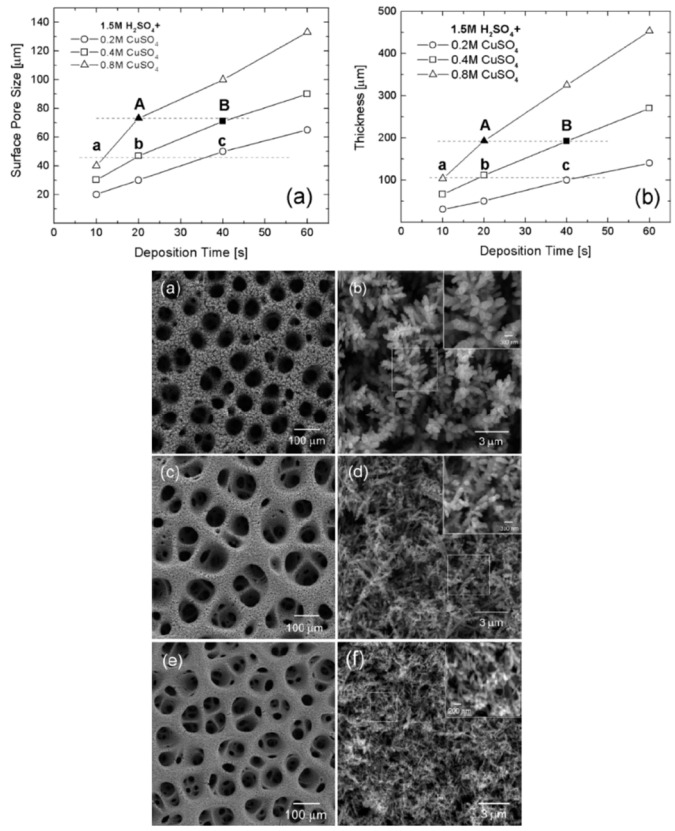

Figure 8. Variation of surface pore size (**a**, **upper left**) and layer thickness (**b**, **upper right**) of electrodeposited Cu in electrolytes with different $CuSO_4$ concentrations. SEM imaging (**down**) of Cu foam electrodeposited for 20 s in an electrolyte containing 0.4 M $CuSO_4$, 1.5 M H_2SO_4, and different amounts of HCL: 1 mM (**a**,**b**), 10 mM (**c**,**d**), and 50 mM (**e**,**f**) [67] (with permission from the American Chemical Society).

The influence of electrolyte components such as NH_4^+, Cl^-, polyethylene glycol (PEG), and 3-mercapto-1-propane sulfonic acid (MPSA) was demonstrated by Kim et al. [69]. Their analysis showed that, among all the additives, NH_4^+ was the most effective suppressant of both Cu deposition and hydrogen evolution, which was due to its adsorption on the electrode surface and the increase in the overpotential of the reactions. This led to a larger pore diameter and lower branching, resulting in mechanically stabilized porous Cu.

Practically important examples of the electrochemical formation of 3D Cu foam that demonstrate the influence of the electrochemical parameters on Cu morphology are summarized in Table 4.

An interesting practical approach for the formation of mechanically stable free-standing porous Cu by means of DHBT has been demonstrated by Kurniawan et al. [70] (Figure 9). This methodology consists of three main steps. During the first step, porous Cu structures are electrodeposited galvanostatically on a flat Cu substrate at current densities in the

typical range for this purpose (i.e., j = −0.075–−2.25 A cm^{-2}) for up to 400 s. In the second step, reinforcement of the obtained Cu dendritic porous structure is performed by applying constant current deposition in the same electrolyte at lower current density (−20 mA cm^{-2}) and longer deposition time (between 5 and 120 min). Because the dendritic reinforcement at the interface between the Cu substrate and porous Cu is less effective, in the third step it is possible to easily detach the porous Cu layer from the substrate by short ultrasonication and finally obtain a stable free-standing porous Cu framework [70].

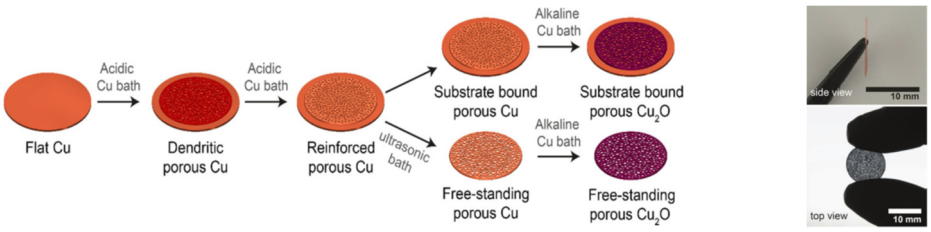

Figure 9. Schematic representation of the electrochemical preparation process of the substrate−bound and free-standing porous Cu and Cu/Cu_2O (**left**) and image showing the free-standing porous Cu (**right**) [70] (open access).

Table 4. Electrochemical deposition conditions and morphology for Cu deposits grown by means of DHBT.

Electrolyte	Electrochemical Parameters	Cell Configuration/ Substrate	Cu Morphology	Ref.
1.5 M H_2SO_4 0.2 M $CuSO_4$	DC galvanostatic max 3 A cm^{-2}	Two-electrode Cu cathode Cu anode	3D microfoam nanostructured walls d_{pore} = 40–100 µm	[71]
0.2–0.8 M $CuSO_4$ 0.1–1.5 H_2SO_4 0.03–0.5 M CH_3COOH 1–50 mM HCl	DC galvanostatic max 3 A cm^{-2}	Two-electrode Cu cathode Pt anode	3D microfoam nanostructured walls d_{pore} = 20–140 µm	[67]
0.3 M $CuSO_4$ 0.7 M H_2SO_4 Additives: $(NH_4)_2SO_4$, HCl, PEG(Mw2000), MPSA	DC galvanostatic 1–4 A cm^{-2}	Two-electrode Cu cathode Cu anode	3D microfoam Wall morph. Depend on additive d_{pore} = 10–40 µm	[69]
0.4 M $CuSO_4$ 0.5 M H_2SO_4 CTAB (10 µM to 5 mM)	DC galvanostatic 0.1–1.2 A cm^{-2}	Three-electrode Au working Pt-counter SCE-reference	3D microfoam nanostructured walls d_{pore} = 50–150 µm; $d_{pore\ (CTAB)}$ = 10–40 µm	[68]
0.5 M $CuSO_4$ 1.5 M H_2SO_4 0.1 M Na_2SO_4	DC galvanostatic 4 A cm^{-2} 2 A cm^{-2}	Two-electrode Cu-cathode Pt-anode	3D microfoam nanostructured walls $d_{pore,\ 2\ Acm^{-2}}$ = 25 µm; $d_{pore,\ 4\ Acm^{-2}}$ = 40 µm	[72]
0.1 M $CuSO_4$ 0.5 M H2SO_4 Add: $(NH_4)_2SO_4$, Na_2SO_4, NaCl, or CTAB	DC galvanostatic 2 A cm^{-2}	Two electrode Cu-cathode Cu-anode	3D microfoam Wall morph. and d_{pore} depend on additive	[73]
0.2 M $CuSO_4$ 1 M H_2SO_4	DC galvanostatic −0.075–−2.25 A cm^{-2} for 60 s and −20 mA cm^{-2} for 2 h (reinforcement)	Three-electrode Cu-working Pt-counter Ag/AlCl-reference	Free-standing porous Cu framework with through pore structure (various d_{pore})	[70]

2.1.5. Summary of Section 2.1

Four different approaches for 3D Cu formation relying on template assistance have been discussed in Section 2.1. These techniques offer final 3D Cu materials with different geometrical forms and dimensions that are strictly controlled by the template geometry. The application of AAO and spherical particle templates can result in the fabrication of ordered Cu structures with near-ideal orientation, i.e., ordered 3D Cu NW arrays and 3D Cu inverse opal, respectively. The utilization of a polymer membrane template enables the formation of Cu NW with random surface distribution and higher diameter variation compared to the AAO approach. One serious challenge in the application of all three solid template approaches is the extra effort necessary for the setting and perfection of the template assembly. In contrast to the solid templates, DHBT does not require additional technological steps to create the template; therefore, this strategy is technologically simpler and more economical. This method allows the formation of 3D-supported or free-standing Cuf layers with micrometer-sized pores that have a disordered spatial distribution and fine surface morphology at the nanoscale, which can be tuned by changing the electrolyte composition. In recent years, simple and low-cost DHBT has gained much attention from the scientific community as a practical approach for manufacturing 3D Cu CCs with high active surface areas, which enable a wide variety of applications.

2.2. Template-Free Methods

Template-free methods for Cu CC structuring do not rely on applying any technique for shape control of the copper deposits. This group of methods comprises more traditional approaches based on anodic electrochemical procedures, i.e., anodization and electrochemical de-alloying, electropolishing, etc.

2.2.1. Electrochemical De-Alloying

De-alloying can be generally classified as a corrosion phenomenon, and has attracted high attention due to the possibility of effectively producing nanoporous metals with a three-dimensional ligament-channel structure. Created in this way, the interconnected material displays an enhanced specific surface area, which makes it suitable for a number of applications, similar to the other types of porous metallic structures. Usually, the necessary materials for the processed bimetallic alloys are prepared via the thermal procedure of powder mixture annealing, which may have a mechanical step as well (e.g., milling, hot-rolling, cold rolling, etc.) [74]. An alternative practical way of alloy formation for certain metal couples is electrochemical deposition [75]. The process of alloy formation is followed by a chemical or electrochemical oxidation step, which has the aim of selectively dissolving the domains of the less noble metal phase (i.e., the metallic component with lower standard electrochemical potential).

The idea for electrochemical de-alloying of Cu alloys dates back to the early 1980s [74,76]. Keir et al. investigated the corrosion process of different binary copper alloys in NaCl solution at various fixed anodic potentials. Cu-Mn, Cu-Zn, and Cu-Ni alloys have shown de-alloying behavior, with the selective loss of Mn able to be optimized by regulating the potential at which the alloy is held [74]. Comprehensive corrosion analysis of Cu-Al, Cu-Mn, Cu-Zn, and Cu-Ni alloys was later performed by Pryor et al. [76]. It was shown that the copper dealloying rate of the binary alloys in NaCl solutions at E = −0.25 vs. SHE decreases in the order Cu-A1 > Cu-Mn > Cu-Zn > Cu-Ni. The properties of the resulting metallic porous structures have been studied as well. Following these early works on electrochemical de-alloying, many possible Cu binary alloys have been investigated, including Cu-Zn [77–79], Cu-Al [80,81], Cu-Zr [82], Cu-Ag [83], and Mg-Cu-Y [84], for effective fabrication of Cu porous materials. The most promising de-alloying results have been obtained for the frequently used copper alloys Cu-Zn and Cu-Al.

The electrochemical de-alloying of Cu-based alloys is usually performed potentiostatically in highly corrosive concentrated chloride [77,78,81,85] or acidic media [82,83]. The chosen de-alloying potential has to be positive enough to selectively dissolve the Cu

alloying element (i.e., Al, Mn, Zn, etc.); however, its value and that of the alloy corrosion potential determine the de-alloying rate.

The evolution of the morphology of porous copper surfaces during Cu-Zn de-alloying in 1-ethyl-3-methylimidazolium chloride (EMIC) electrolyte was studied by Lin et al. [77] through SEM imaging. As the de-alloying process began, Zn atoms were selectively removed from the alloy surface, followed by pitting. It was found that the dissolution of Zn from the alloy begins preferentially at the grain boundaries. As de-alloying proceeds, this selective dissolution of Zn leads to Cu enrichment, finally resulting in larger ligaments and increased pore size. A similar morphological pattern has been observed for products obtained in other electrolytes.

2.2.2. Anodic Treatment of Cu Substrate

Anodic electrochemical treatment comprises a group of methods that can be used to modify the morphology of the metal surface, or, depending on conditions, to promote formation of an oxide layer, which can be useful for different functional applications. In this section, the most frequently used anodic treatments of copper substrates, namely, anodization, and electropolishing, are briefly discussed.

Anodization

Anodization is an electrochemical passivation process applied to increase the thickness of the natural oxide layer on certain metal surfaces. The process received its name because it is performed under constant anodic potential, constant positive current, or anodic linear polarization, leading to oxidation of the metal surface and corresponding oxide formation. The anodization technique is often used to passivate Al or Ti and obtain Al_2O_3 and TiO_2 layers for different purposes. In addition to this frequent use, other metals, including Cu, have been anodized.

Reyter et al. [86,87] demonstrated that a nanostructured and highly electrocatalytic surface can be obtained by anodization of a polycrystalline copper electrode in 1 M NaOH. They showed that this process results in the formation of $Cu(OH)_2$ nanorods on the Cu surface. These nanostructures can then be thermally reduced under H_2 atmosphere and converted to metallic copper nanowires with a rough nanostructure surface. The same approach was applied by Wang et al. [88] for the formation of Cu nanowires on Cu foam. (Figure 10).

Chen et al. [89] prepared core–shell $Cu@Cu_6Sn_5$ nanowires with a three-dimensional structure through an electrodeposition process using $Cu(OH)_2$ nanostructures obtained by anodization of the Cu substrate. Anodization was performed in 1 M NaOH aqueous solution under a constant current of 8 mA and at room temperature. The anodized Cu foil prepared in this way was used for electrodeposition of the Sn–Cu composite [89].

Anodic Treatment in Acid Electrolytes

Pauric et al. [90] demonstrated that a Cu surface with a regular morphology and a porous structure at the sub-micrometer scale can be obtained by anodic treatment of highly concentrated phosphoric or sulfuric acids. This approach requires a very viscous electrolyte with sufficient conductivity. Essential for this method is the presence of a small residual amount of water and a sufficiently high voltage to provide an intensive oxygen bubble evolution. Furthermore, it has been demonstrated that the thickness of the porous layer can be flexibly scaled up to over one micrometer and that the formation process can be performed independently of substrate purity or crystallographic features [90].

Figure 10. Fabrication of Cu NW-Cu current collector: (**a**) schematic illustration showing the preparation process of Cu nanowires and their in situ growth on Cu foam along with SEM images of (**b**) bare Cu foam, (**c**) CuO NW-Cu, and (**d**) Cu NW-Cu [88] (with permission from Elsevier).

Another original electrochemical approach for tuning the morphology of structured Cu was proposed by Pham et al. [91]. They reported a complex strategy for controllable modulation of multiple parameters, including porosity, wetting properties, and transport, by applying different electrochemical steps. In particular, hierarchically designed copper inverse opal was created for enhanced liquid transport through the pores. This step was followed by electropolishing to systematically modulate the structural porosity. Finally, electrodeposition of the oxide layer and further electrochemical oxidation enabled functionalization of the porous structure [91].

2.2.3. Summary of Section 2.2

Template-free methods for 3D Cu CC formation do not involve the use of any techniques for shape control of the copper deposits, which makes these approaches generally uncomplicated. By means of electrochemical de-alloying, a three-dimensional ligament-channel 3D Cu structure can be obtained. Materials created in this way offer a large specific surface area, which is typical for the other types of 3D Cu CCs as well, enabling several potential applications. Critical aspects of this method involve the alloy's composition and structure and the de-alloying potential, fine-tuning of which are essential for the structural morphology, physical properties, and composition of the obtained 3D material. These challenges limit the easy and straightforward practical application of these methods to a certain extent, as strict control over those parameters is necessary.

Depending on the electrolyte media, anodic treatment of the pure Cu phase provides additional possibilities for structuring and modification. In particular, anodization of already-formed 3D Cu CCs in alkaline media results in the formation of $Cu(OH)_2$ with a nanomorphology that can be further chemically modified. Alternatively, anodic treatment of Cu in a highly concentrated acidic solution can be used to obtain sub-micrometer porosity for modulation of the fine surface morphology of 3D Cu materials synthesized by other methods.

3. Electrochemical Characterization of 3D Cu CCs

3D micro- and nanostructured materials display a number of properties that make them favorable for multiple applications, including energy conversion and storage. Traditionally, structured Cu materials are physically and electrochemically characterized to reveal their active surface area, porosity, mechanical and electrochemical stability, and

electrical properties. Additionally, the ionic transport of different chemical species in 3D structured materials is important in electrocatalytic and energy storage applications. In this section, a number of electrochemical methods for 3D Cu characterization are discussed, including both popular and unconventional approaches. Please note that the characterization of 3D Cu materials by means of physical and spectroscopic methods is outside the scope of the current review paper.

3.1. Electrochemical Stability

The electrochemical stability of current collectors is important for their normal operation in relation to the particular application where they are planned. In water-based electrolytes, copper anodic stability is limited by its oxidation, which leads to complete dissolution in acid media (pH < 3; E^0 = 0.34 V vs. SHE) or to the formation of $Cu(OH)_2$ in alkaline solutions (pH > 12). In the intermediate pH region (3 < pH < 12), the electrooxidation of metallic Cu yields a Cu_2O layer. Furthermore, it has to be taken into account that the oxidation potential of Cu depends on the solution acidity. At pH < 3, Cu dissolves at a constant potential, while with a decrease in acidity the equilibrium potential of Cu drops significantly ($E^0 = -0.25$ at pH = 12) [92]. In order to study the electrochemical stability of Cu in water-based electrolytes, the equilibrium potential can be measured against known reference electrodes; further, the redox behavior of Cu can be investigated by voltammetry in the particular electrolyte composition. The discussed potential shift is evident in voltammetric measurements of electrolytes with differences in pH [92].

Cu CCs have numerous applications that involve operating in non-water-based electrolytes, e.g., in Li ion organic solutions. Therefore, the electrochemical stability of Cu in organic-based media is an important property. Definite differences in the electrochemical performance of Cu CCs can be observed in organic electrolytes, in the absence of water. For example, in Li ion organic carbonate-based electrolytes, Cu CCs start to dissolve intensely at about E = 3.5 V vs. Li or Li^+ electrodes. Compared to this behavior, Cu shows a minor redox activity in [EMIm][TFSI] and [BMIm][TFSI] ionic liquid electrolytes, which may be beneficial for increasing the safety of lithium-ion batteries, especially in the over-charged state [93].

3.2. Surface Area

The electrochemically active surface area (A_{ECSA}) is an important characteristic of active materials and supports suitable for electrocatalysis and energy storage applications. There are a number of electrochemical strategies for determining the A_{ECSA} of metallic nano- and microstructured electrode materials. Nevertheless, the particular determination of the A_{ECSA} of Cu structured materials remains underexplored.

Cyclic voltammetry was applied by Giri et al. to electrochemically estimate the A_{ECSA} of copper powder [94]. Three CV approaches were applied to assess the A_{ECSA} of the electrode material, including (1) voltammetric stripping of a UPD-deposited Pb monolayer, (2) by means of the double-layer capacitance obtained by CV, and (3) by voltammetric analysis of surface monolayer oxide formation.

3.2.1. Underpotential Deposition of Pb

The UPD method is an electrodeposition process of metal atoms of one metal onto a surface of another metal; it can take place at potentials more positive than the equilibrium potential, and is typically limited to only one monolayer. This phenomenon is an interesting demonstration of a stronger binding of the metal atom to the foreign substrate than to its own bulk phase. Many studies on the UPD of relatively active elements on noble metal surfaces (e.g., Au, Pt, etc.) can be found in the literature [94–96]. Characteristically, lead atoms can be underpotentially deposited on copper surfaces [94]; thus, the A_{ECSA} of copper can be assessed using the charge passed due to the deposition or dissolution processes. Bulk and UPD Pb deposition and dissolution phenomena are presented on the voltammogram in Figure 11, left. The Pb monolayer stripping charge can be used to

estimate the A_{ECSA}. The charge areal density during the UPD process depends strongly on the crystal planes presented on the substrate surface. In the case of polycrystalline copper, an equal contribution from the three basic planes (1 0 0), (1 1 0), and (1 1 1) can be assumed; therefore, the average charge amount corresponding to one monolayer is 250 μC/cm^2 [94].

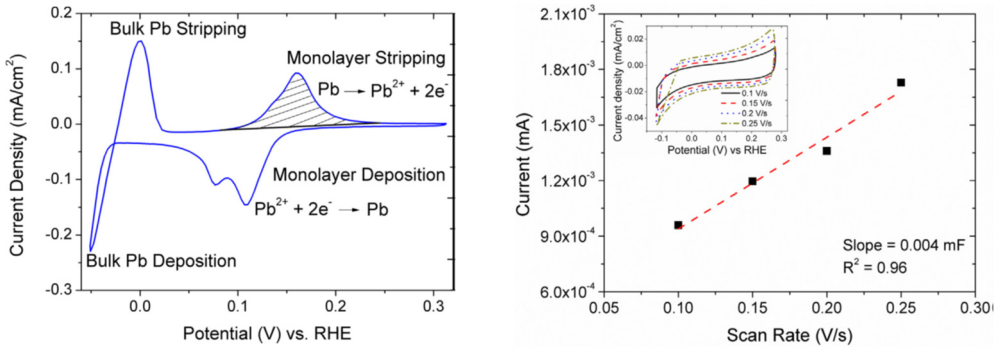

Figure 11. Cyclic voltammetry of copper powder in Ar-saturated 0.01 M $HClO_4$ + 1 mM $PbCl_2$ solution at a scan rate of 10 mV/s (**left**) and plot of the double layer current vs. scan rate (**right**). The slope of the straight line is the capacitance in mF. The insert in the right figure shows the cyclic voltammograms of the drop-cast copper powder electrode in Ar-saturated 0.1 M $HClO_4$ solution at a scan rate of 100 mV/s, 150 mV/s, 200 mV/s, and 250 mV/s [94] (with permission from Elsevier).

3.2.2. Double-Layer Capacitance

The capacitive surface charge/discharge phenomenon of the electric double layer (EDL) in the electrolyte solution can be applied for the A_{ECSA} assessment [94,97]. The EDL capacitance depends on the A_{ECSA} of the electrode material and its physical properties (dielectric constant). For the purpose of A_{ECSA} evaluation by cyclic voltammetry, curves at different scan rates have to be obtained in an acidic solution (e.g., 0.1 M $HClO_4$) in the absence of the Faradaic reaction (Figure 11, right). EDL capacitance (dQ/dE) can be calculated from the slope of the current vs. the scan rate dependence. After the estimation of EDL capacitance, the A_{ECSA} can be determined by dividing the acquired EDL capacitance value by the surface area-specific reference capacitance value (C_{ref} = 28 μF/cm^2) [94].

3.2.3. Cu Electro-Oxidation

The electrochemical oxidation of Cu in alkaline solution results in the successive formation of Cu_2O, CuO, and $Cu(OH)_2$. These oxygen-containing products can be reversibly reduced back to copper. The first redox process during the oxidation CV scan corresponds to Cu_2O formation [94]. For estimation of the A_{ECSA}, it can be assumed that the formation of Cu_2O proceeds in the form of a monolayer. It has been determined that the charge density factor (charge per unit surface area) for the formation of the Cu_2O monolayer is 352 μC/cm^2 [94,98,99].

Zankowski et al. [100] compared different methods for evaluating the A_{ECSA} of Ni nanomesh obtained by the AAO template method, including voltammetric analysis, impedance spectroscopy, and BET. Their results are summarized in Figure 12. A linear increase in the voltammetric charge, peak current, and EIS double-layer capacitance with the thickness of the nanomesh and its surface area was observed. The highest accuracy in determining the surface area is provided by the method based on electrochemical surface oxidation and the double layer capacitance, for which the A_{ECSA} assessment is in good agreement with that obtained by geometrical modeling and BET [100] (Figure 12).

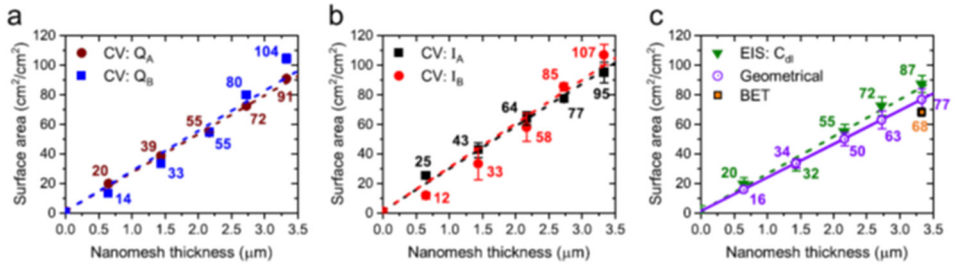

Figure 12. Nanomesh surface area analyzed using (**a**) CV charge, (**b**) CV current, and (**c**) EIS double layer capacitance together with the geometrical and BET surface area [100] (open access).

3.3. Porosity

Porosity is a central property of structured current collectors, and is directly related to their function as electrodes. It can be defined as the ratio of the real pore volume V_{pore} to the total geometrical volume of the material V_{total} (Equation (1)). On the other hand, V_{total} is the sum of V_{pore} and the volume of the structured solid metal V_{solid}, which corresponds to the volume of the nanowires, nanofoam, or any specific Cu nanostructure. Therefore, the porosity P can be calculated using the following expression (Equation (1)).

$$P = \frac{V_{pore}}{V_{total}} \cdot 100 = \left(1 - \frac{V_{solid}}{V_{total}}\right) \cdot 100 \quad (1)$$

If the structured material forms a homogeneous layer with constant thickness, its V_{total} can be easily determined by measuring its thickness. V_{pore} can be calculated from the relation $V_{pore} = V_{total} - V_{solid}$, where the volume of the nanostructure V_{solid} can be estimated Coulometrically from Faraday's law using its deposition or dissolution charge [100].

3.4. Ionic Transport

An accelerated level of ionic transport, i.e., high ionic conductivity, in the porous structure is an essential condition enabling normal electrode operation in any electrochemical application. It is, however, challenging to precisely evaluate the ionic conductivity in porous materials, as porous electrodes are involved in different parallel phenomena that affect the total impedance of the structure. These include, for instance, (i) mixed conduction with both electron and ion species, modeled as electric resistance (R_e), electrolyte bulk resistance (R_{sol}), and ionic resistance in pores (R_{ion}); (ii) electric double layer charging (C_{dl}); (iii) charge transfer due to redox process (R_{ct}); and (iv) mass transport of electroactive species [101–104].

To overcome this challenge, de Levie et al. built a theoretical impedance model for the interpretation of cylindrical porous system impedance, which they developed and applied to different conductive porous electrodes filled with electrolytes [101–104]. Their theoretical approach was based on transmission line models (TLMs), which have equivalent circuits for non-Faradaic and Faradaic processes, as presented in Figure 13. The corresponding impedances can be modeled using the following equations, (Equations (2) and (3)) [101].

$$Z_{nonfaradic} = \sqrt{\frac{R_{ion,L}}{j\omega C_{dl,A} 2\pi r}} coth \sqrt{R_{ion,L} j\omega C_{dl,A} 2\pi r} L \quad (2)$$

$$Z_{faradic} = \sqrt{\frac{R_{ion,L} R_{ct,A}}{(1 + j\omega R_{ct,A} C_{dl,A}) 2\pi r}} coth \sqrt{\frac{R_{ion,L}(1 + j\omega R_{ct,A} C_{dl,A}) 2\pi r}{R_{ct,A}}} L \quad (3)$$

The ionic resistance R_{ion} in the pores can be obtained by extrapolating the impedance signal towards the low-frequency limits, (Equations (4) and (5)):

$$Z_{nonfaradic,\omega \to 0} = \frac{R_{ion}}{3} \quad (4)$$

$$Z_{faradic,\omega\to 0} = \frac{R_{ion}}{3} + R_{ct} \quad (5)$$

where $Z_{nonfaradic}$ and $Z_{faradic}$ are the impedances of the pore in case of the absence and presence, respectively, of Faradaic reaction, C_{dl} is the double-layer capacitance, R_{ct} is the charge transfer resistance and L—the pore length.

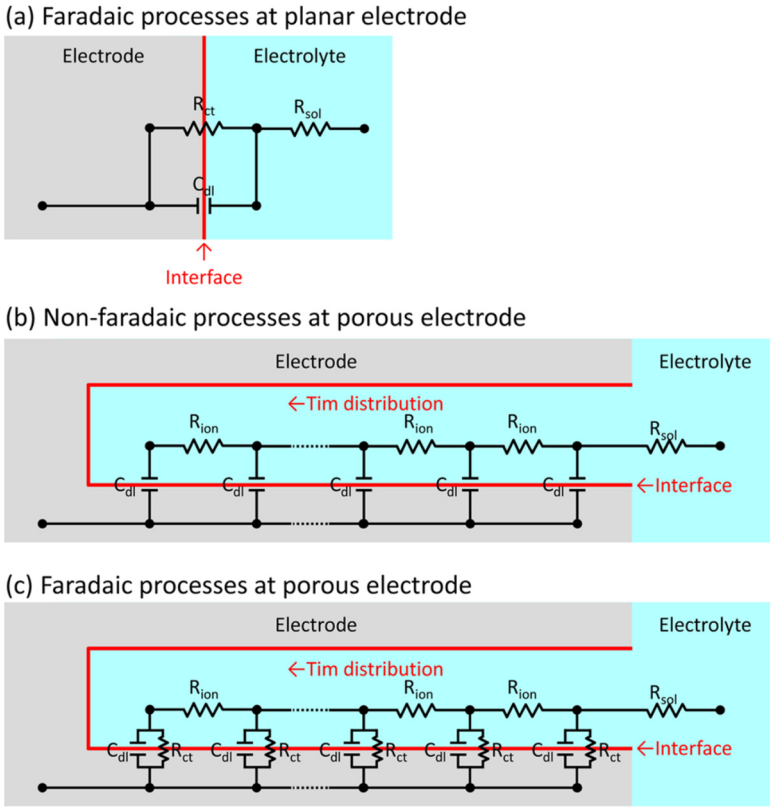

Figure 13. Schematic representations of electrode structures and their equivalent circuit models [101] (with permission from the American Chemical Society).

To the best of our knowledge, this theoretical approach for the evaluation of R_{ion} has not yet been applied to Cu porous systems.

3.5. Summary of Section 3

The possibilities for electrochemical characterization of practically relevant 3D Cu CC properties are currently underexplored. Electrochemical stability, surface area, porosity, and ionic transport in the 3D Cu structure are properties that can be evaluated electrochemically using simple and available techniques. While only scarce data about the specific surface area of 3D Cu and its porosity are available in the literature, investigation of the ionic transport in 3D Cu has, to the best of our knowledge, not yet been studied. A_{ECSA}, P, and R_{ion} are important parameters for the practical application of 3D Cu CCs; additional knowledge about ways to measure them would permit more efficient application of 3D Cu CCs and allow better modeling of the relevant processes.

4. Application of Structured Cu CCs in Energy Conversion and Storage

In this section, the most important applications of electrochemically obtained structured Cu CCs in the field of energy conversion and storage are presented. In this growing field, relevant battery, capacitor, and electrocatalytic applications are considered. Where possible, the usefulness of the relevant Cu CC formation techniques compared to alternative methods is discussed.

4.1. Electrocatalysis

Cu CCs can play a key role in certain electrochemical devices that are based on electrocatalytic reactions. Cu is highly conductive and can be used to provide fast electron transfer in an electrochemical system. The implementation of Cu CCs is mainly effective when used as a negative electrode, i.e., at relatively low potentials. This is because Cu metal dissolves easily into Cu^{2+} when used as a positive electrode, especially in acidic electrolytes ($E^0 = -0.34$ V vs. SHE). In Li ion organic electrolyte, its dissolution starts at E = 3.5 V vs. Li, Li^+. This redox behavior is associated with the lack of a stable passive oxide layer formed on the Cu surface, which could be able to protect the metal from further bulk oxidation. As a result of these redox properties, the application of Cu CCs is limited to a relatively narrow potential range. Several of the interesting and important applications of Cu CCs are discussed below.

In several of these applications, structured Cu CCs are used as substrates and coated with an active catalyst, which lowers the overpotential for the electrochemical reaction and consequently enhances the efficiency of the electrochemical devices. In this case, the catalysts used to trigger and accelerate the electrochemical reactions are selected based on the application.

4.1.1. Hydrogen Evolution Reaction (HER)

In recent years, the development of catalysts for HER has been growing significantly. Among these catalysts, noble metals such as Pt are acknowledged as the benchmark due to their low overpotential and high efficiency towards the HER [105]. The use of 3D nanostructured Cu foams allows the catalyst to be deposited in low amounts, while preserving its high catalytic performance due to the increased active surface area.

An interesting approach was conducted by Rezaei et al. [106], who deposited a bimetallic Pt/Pd catalyst on Cu foam with dendritic pore walls using a galvanic replacement reaction method. This approach has the advantage of replacing the Cu atoms with Pd and/or Pt only at the surface, realizing a very low and self-limiting thickness of the catalytic material. In this way, a thin and homogenous layer of the metal coating can be achieved. $Pd_{65}Pt_{35}$ catalysts with a bimetallic layer have shown promising results by lowering the overpotential of the HER, as shown in Figure 14. Pristine Pt and Pd coatings exhibit an overpotential of 240 mV and 51 mV for HER, respectively, while the bimetallic $Pd_{65}Pt_{35}$ electrode displays a remarkably low overpotential of only 5 mV. The observed strong catalytic effect is associated with the high catalytic activity of the Pt/Pd bimetallic layer, and is accelerated by the extremely high surface area of the Cu foam.

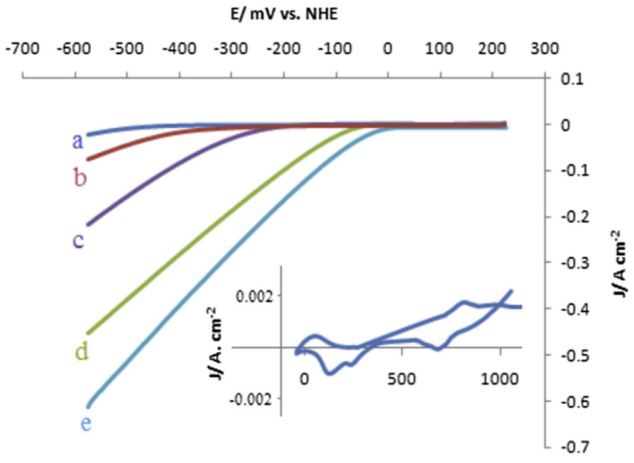

Figure 14. Linear scan voltammogram of different electrodes: (a) planar Cu, (b) Cu nanofoam, (c) Pd on Cu nanofoam, (d) Pt on Cu nanofoam, and (e) Pd65Pt35 on Cu nanofoam. The experiments were

performed in 0.5 M H_2SO_4 solution at a scan rate of 50 mV s^{-1}. The inset shows cyclic voltammograms of $Pd_{65}Pt_{35}$ on a Cu nanofoam electrode in the same electrolytes at a scan rate of 10 mV s^{-1} [106] (with permission from Elsevier).

Providing a replacement material that can represent an alternative to expensive noble metals is an essential part of reducing the overall production cost of HER electrodes. This economically useful strategy was explored by Das et al. [107], who used Ni-based alloys such as nickel phosphide (Ni_5P_4) as an electrocatalyst. A single-phase Ni_5P_4 catalyst is less expensive compared to pure noble metals; furthermore, Ni_5P_4 can be electrodeposited on a Cu foam substrate using the galvanostatic method [107]. The increased surface area of the Cu foam helps to improve the charge and mass transfer, which in turn significantly enhances the catalytic performance. The deposition of Ni_5P_4 catalysts on a Cu foam electrode achieved a low overpotential of 160 mV for the HER, which is considerably lower than the achieved with the deposition of Ni_5P_4 catalysts on other substrates. These results reveal the importance of structured Cu foam in enhancing electrochemical activity, such as the adsorption of the H^+ ions for the hydrogen evolution reaction [107].

4.1.2. CO_2 Reduction

In recent years, there has been growing interest in research on electrochemical CO_2 reduction due to the rising environmental risk from increasing CO_2 concentrations in the atmosphere. For this application, Cu is considered the only metal able to electrochemically convert CO_2 into C1 (methane and methanol), C2 (ethylene and ethyl alcohol), and even C3 (propane, propylene, and propyl alcohol) products [108]. Several investigations have aimed to better understand the selectivity of the Cu catalysts in obtaining these products. It was later discovered that product formation depends on the facet's orientation with respect to the Cu surface [109]. The C1 pathway is preferential on Cu(111) surfaces, while the C2 pathway is more likely to generated products on Cu(100) surfaces due to higher C-C coupling activity attributed to the higher binding energy of adsorbed *CO on Cu(100) facets compared to Cu(111).

The implementation of Cu foam as a catalyst and electrode for CO reduction was summarized by Vestergom et al. [108], where quantification of the CO_2 reduction products at different current densities on a flat Cu wafer and Cu foam was presented (Figure 15).

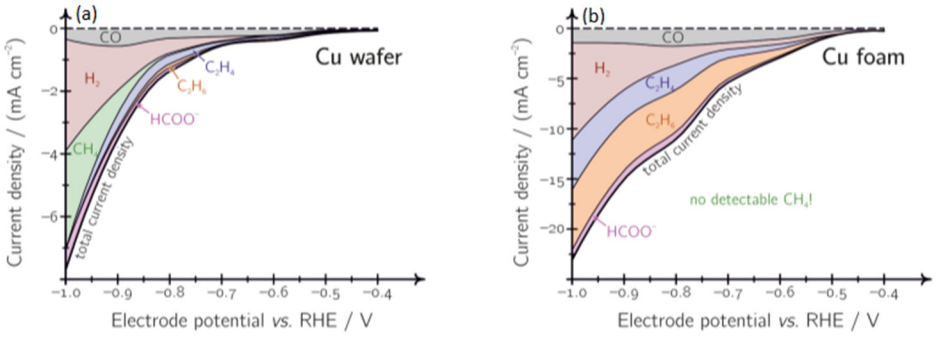

Figure 15. Polarization curves (interpolated) of (**a**) copper wafer and (**b**) copper foam with a deposition time of 20 s. The experiments were performed at distinct potentials in a CO_2-saturated 0.5 mol dm^{-3} $NaHCO_3$ solution, and product quantification was determined by an online gas as well as by post-electrolysis ionic liquid chromatography [108] (open access).

The high surface area of Cu foam significantly increases the current density, resulting in a higher number of products, and generates higher selectivity towards ethylene (C_2H_4) and ethane (C_2H_6) formation, with a combined Faradaic efficiency (FE) of 55% at a fixed voltage of −0.8 V vs. RHE. This is mainly influenced by the pore size diameter of the foam structure, as well as by its thickness. Dutta et al. [108] identified temporal trapping of gaseous intermediates such as CO, H_2, and C_2H_4 inside the dendritic mesoporous structure, which enhances the selectivity with respect to C2 products.

Another fascinating innovation for this application is the use of a highly ordered copper inverse opal structure (Cu-IO) by Song et al. [59]. The structured Cu-IO was synthesized using a polystyrene (PS) bead template with different layer thicknesses on a sputtered Au substrate. The six-layered Cu-IO generated the highest FE for C2 products such as ethylene (at ~30%) and ethanol (at 10%) when applied at a fixed potential of 0.8 V vs. RHE. Though an increased number of layered Cu-IO (up to twelve layers) reduced the overpotential of the generated gas products due to the enhanced active surface area, these structures did not improve the overall selectivity or FE. In comparison with Cu foam, the selectivity and concentration with respect to C2 products were superior to those of Cu-IO.

4.2. Energy Storage

Energy storage is possibly the most frequent electrochemical application of structured Cu CCs. In this section, the most significant types of structured Cu CC applications are briefly summarized, and the role of the different technologies for Cu CC fabrication is discussed. The crucial Cu CC properties that are essential for energy storage applications are the porosity and the electroactive surface area. The parallel increase of these parameters has enabled efficient electrochemical process by accelerating both charge transfer and ionic transport. The methods presented in Section 2 for structured Cu CC formation provide a number of excellent possibilities for increasing active surface area and porosity while at the same time enhancing the mechanical stability of the deposited active materials during ion insertion reaction by reducing the accumulated internal stress.

The utilization of 3D Cu CCs for diverse electrochemical energy storage applications can be categorized by relevance to the specific electrode function, including (a) active electrode materials, (b) 3D scaffolds/templates, and (c) conductive substrates/current collectors [2]. In this work, in order to compare the different Cu formation methods, the focus has been on the most popular uses of Cu CCs, namely, as anodes in Li ion batteries and supercapacitors.

4.2.1. In Li Metal Battery Anodes

Li metal has the highest capacity as an anode material for Li ion batteries. However, the high reactivity of Li, its large volume changes, and fast Li dendrite formation greatly affect the performance and safety of Li metal batteries. Therefore, the most serious challenges in this field are low Coulombic efficiency and uncontrollable Li dendrite formation [110–112]. One original solution to the problem of Li deposition is to influence the nucleation and growth of Li by application of 3D structured Cu CCs, which provide the following benefits: (1) reduced local current density, (2) slowing mossy and dendritic growth of Li, and (3) buffering the volume change during Li metal growth. This idea has been realized by the application of structured 3D Cu CCs, mostly obtained by means of DHBT [113–116] and less frequently by the AAO template [31,117], inverse opal [118], and electrochemical de-alloying [78,119] techniques.

The DHBT approach has displayed the most visibly positive effects from structured 3D Cu CCs, which is probably associated with the resulting very high active surface area. Chen et al. [114] applied a self-supporting dendritic copper porous film formed with the assistance of hydrogen bubbles as the substrate for Li plating/stripping. It was found that Li initially forms uniformly on the surface of Cu nanoparticles and grows laterally along Cu dendrites, which results in filling the pores of the 3D Cu CC. In this way, the vertical growth of Li dendrites is effectively inhibited. This allows successful cycling with a high current density (up to 3 mA cm^{-2}), a high real capacity of 6 mA h cm^{-2} of the anode, high Coulombic efficiency of 98%, and long cycling stability over 2400 h (i.e., 1200 cycles) [114]. Comparably positive results were obtained by Qiu et al., who used the same DHBT approach [113] (Figure 16).

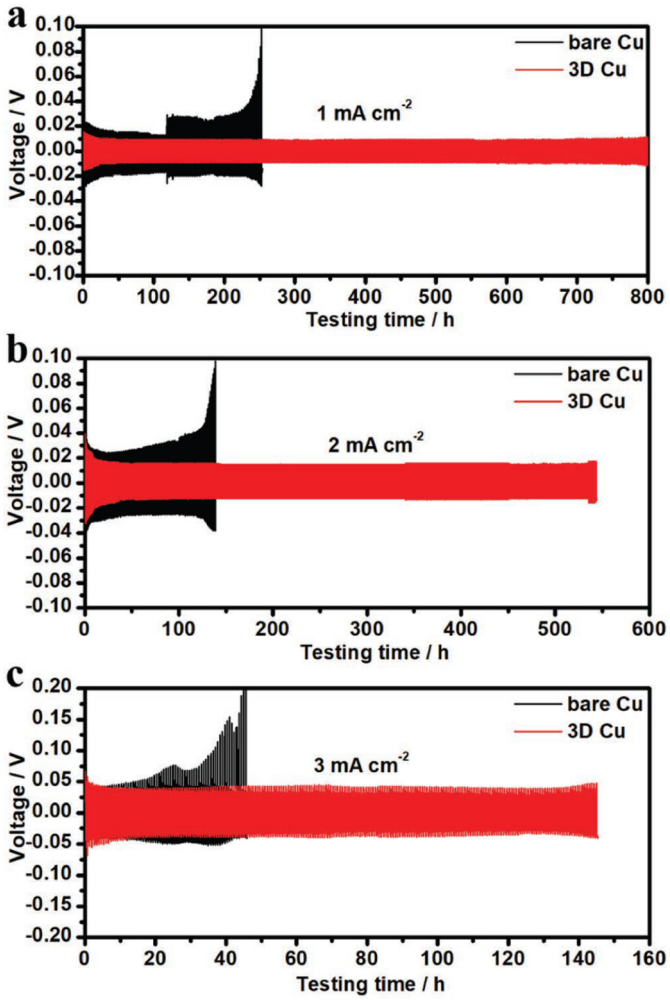

Figure 16. Cycling performance in symmetrical Li | Li-3D Cu and Li | Li-Cu cells. Voltage–time profiles at (**a**) 1, (**b**) 2, and (**c**) 3 mA cm^{-2} with a cycling capacity of 1 mA h cm^{-2} [113] (with permission from Wiley).

Tang et al. [120] demonstrated the unique structural benefits of a 3D structured Cu current collector formed by self-assembly using a PMMA spherical particle template. The anode based on this structure can operate stably for 750 h at 0.2 mA/cm^2 with a very small Li electroplating/stripping overpotential (<30 mV) and up to 93.3% Coulombic efficiency over 120 cycles [120]. Although somewhat less effective than the simple DHBT approach, the particle template strategy demonstrates the high performance of 3D Cu nanostructures for Li plating stripping. Using the same PMMA particle template, the performance of the resulting inverse opal structure was enhanced by pulse electroplating with a lithiophilic Zn layer. In this way, an improved rate performance of the 3D Cu CC for Li metal deposition at current densities of 0.2, 0.5, 1.0, and 2.0 mA cm^{-2} was demonstrated [118].

A few works on electrochemical dealloying [78,119] have presented very competitive results as well. Using this method, Zhao et al. prepared a compact 3D Cu current collector with a uniform porous structure for Li metal batteries using an easily controllable and low-cost voltammetric etching approach with Cu–Zn tape. The anode showed stable cycling for at least 400 h under high Li utilization (1 mA h cm^{-2}) and a high current density of 1 mA cm^{-2}. Furthermore, the 3D Cu | | $LiFePO_4$ full cells displayed excellent cycling and rate performances as well [119].

Another interesting though technically more challenging approach is the application of the AAO template method to obtain the Cu nanostructure followed by transformation to a lithiophilic hyperbranched Cu_xO nanostructure. This type of surface modification

permits Li deposition with minimal nucleation work, which induces more homogeneous Li nucleation and growth. Consequently, the nanostructured Cu@CuxO anode displays a low Li deposition overpotential of 44.3 mV, high Coulombic efficiency of 98.33%, and good rate performance, which allows current densities up to 5 mA/cm^2 to be applied [117]. Thanks to the benefits of this modification, Cu structures obtained by the AAO template method can compete with the cycling performance of materials formed by the DHBT and electrochemical de-alloying techniques. Nevertheless, the technical simplicity of DHBT remains an important advantage.

It has to be noted that the 3D Cu CC structure alone is not a universal solution to the problem of insufficient anode performance in Li metal batteries. On the one hand, the implementation of 3D Cu CC can improve the Li deposition and cycling stability of Li metal battery anodes. However, due to side reactions between the Li and electrolyte, the increased exposed interfacial area of the 3D Cu CC results in enhanced depletion of the electrolyte and accelerated consumption of the Li metal inventory. Therefore, in real battery conditions improving the anode performance is only possible by simultaneously stabilizing the Li plating and circumventing the side reactions that reduce anode efficiency and lead to depletion of the electrolyte. Thus, there is intensive ongoing research into the development of stable and efficient electrolytes for Li metal batteries [121].

4.2.2. 3D Cu CCs for Si Anodes in Li Ion Batteries

The cycling performance and in situ mechanical stability of many anode materials used for energy storage, e.g., Si. Sn, NiP, and different TMOs, can be improved by using 3D structured porous substrates as current collectors. Among these examples, the mechanical stabilization and performance improvement of Si when used as an anode material has been the aim of a large number of works. In this context, Si electrodeposition in DHBT-formed Cu is one original recent approach [122–124].

In this application, Si is electrochemically deposited on free-standing porous Cu deposited by the DHBT method [124]. The authors concluded that the porous morphology of the substrate and the composition of the electrolyte used for Si deposition have a combined impact for the improved electrode performance. The best electrochemical properties in terms of specific capacity, rate capability, and long-term cycling were observed for Si deposited using sulfolane electrolyte in a p-Cu substrate, specifically, a stable reversible capacity of 2500 mAh g^{-1} during the first 250 cycles and promising capacity retention (Figure 17). The authors attributed this positive effect to the improved mechanical stability of the active material and to accelerated ionic transport in the porous structure of the anode. Cycling performance approaching these values has been presented by Suk et al. as well [122].

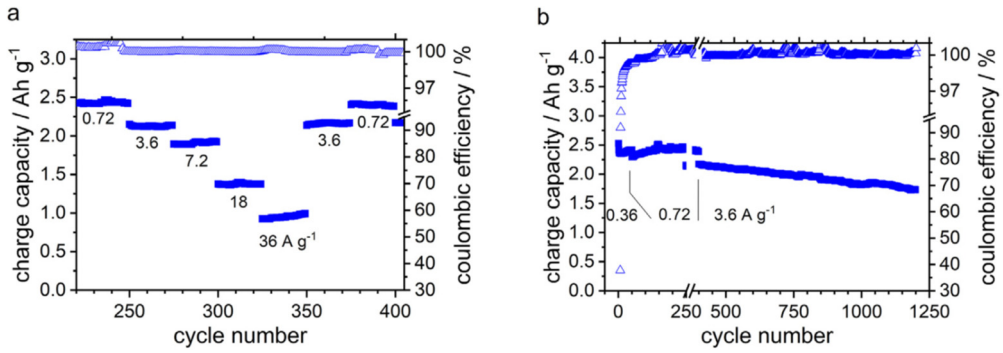

Figure 17. Evolution of charge capacity of a p-Cu/SL electrode at different current densities (**a**) and long-term galvanostatic cycling (**b**) [124] (with permission from Elsevier).

4.2.3. Supercapacitors

3D structured copper, particularly copper foam obtained by DHBT, has been investigated as an active material for supercapacitors. A Cu(II)/Cu(0) reversible surface redox

couple has been considered as an active process responsible for the pseudocapacitance. Mirzaee et al. [125] studied the influence of the morphology and porosity of dendritic Cu structures tuned by means of acetic acid as a hydrogen bubble stabilizer on the measured capacitance. After structural 3D Cu foam optimization, capacitance values reaching 102.7 F g^{-1} were obtained, with capacitance retention of 90% after 6000 cycles at a cycling current density of 20 mA cm^{-2}.

An improvement in the cycling performance was observed after replacement of the Cu foam with a bimetallic Ni–Cu foam. In this case, the pseudocapacitive behavior was associated with the reversible Ni^{3+}/Ni^{2+} redox couple [126]. Additionally, Lange et al. demonstrated significant improvement in capacitance when an electrodeposited Cu–Fe composite foam was used [127]. These examples demonstrate that DHBT-derived Cuf has the potential to be utilized as the active material for supercapacitors with sufficiently good performance. However, there is scope for including new functional properties, as well as for precise adjustment and modification of the nanostructure for applications in other fields involving energy storage systems.

4.3. Summary of Section 4

3D electrochemically structured Cu CCs are employed in electrocatalytic and energy storage applications, including HERs, CO_2 reduction, anode CCs in rechargeable batteries (mostly LIBs), and supercapacitors. The positive effects of 3D Cu CCs are associated with their large surface area and micro-/nanoporous structure. This enables the local current density and reaction overpotential to be reduced. Furthermore, nanostructured Cu CCs can provide mechanical stabilization of the coated active materials during ion insertion and, in parallel, shortening of the diffusion length of the electroactive species, resulting in more efficient battery anode operation. DHBT currently dominates the research on electrochemical applications of this material, as it is a simple and low-cost strategy for 3D Cu CC formation.

5. Conclusions and Outlook

There are multiple methods for the formation of 3D Cu CCs that find practical application in many fields of research and technology, primarily as current collectors in electrochemical energy storage and electrocatalysis. Among these strategies, electrochemical techniques offer useful alternative solutions in terms of higher technical flexibility, simplicity, and cost reduction, attracting the attention of many researchers and development engineers. This review provides a systematic analysis of the electrochemical methods for 3D Cu CC formation, an overview of the main electrochemical approaches for the characterization of the most relevant functional 3D CCs properties, and useful examples of their application. Based on a comprehensive analysis of the available literature, the following concluding statements can be formulated:

- The most frequently used and important electrochemical methods for 3D Cu CC formation are presented. This comprises a brief overview of the methodological principles, followed by examples illustrating the conditions for their particular implementation (i.e., experimental setup, electrochemical parameters, electrolyte composition, and product morphology). Thus, the displayed information enables straightforward application of these strategies by a broad range of specialists in the field.
- DHBT is the simplest and most economical 3D Cu CC formation technique in comparison to the alternatives, which require template assembly and additional technological steps. This method utilizes relatively high deposition currents, essential for the intensive HER, which might require extra current boosting of the conventional potentiostat/galvanostat devices. Furthermore, a second dendrite reinforcement step is necessary to achieve better mechanical stability of the structure, which offers the possibility of forming free-standing 3D Cu CCs. The large active surface area of 3D Cu CCs with dendrites is highly beneficial for energy conversion and sensing devices, while due to their reinforced mechanical strength free-standing 3D Cu CCs provide

unique features that can be utilized in closed and compact cells, e.g., battery cells (cylindrical, coin, and pouch cells) and/or stack electrochemical cells (electrolyzer or reduction cells). The formation of free-standing 3D Cu CCs opens up new possibilities for the development of various interesting electrochemical applications.

- Electrochemical characterization of the active surface and porosity of 3D Cu CCs is a simple and low-cost approach. However, it remains an underexplored area in terms of establishing the limits of these methods for the analysis of different 3D Cu types. In order to associate the functional behavior of 3D Cu CCs with their structural properties, quantitative data about the electrochemically active surface area, porosity, and ionic transport in the porous structure are required. This can assist in comparing materials obtained by different methods and make analysis less empirical.
- Electrochemically obtained 3D Cu CCs have demonstrated their application in multiple fields, including Li ion batteries, HER, CO_2 reduction, etc. The 3D Cu structures formed by means of the DHBT, AAO template, and electrochemical de-alloying methods present comparable performance as CCs for anodes in Li metal batteries. However, owing to its simplicity, the DHBT approach is more frequently applied, and is preferred for research. Electrochemically structured 3D Cu CCs enable reduction of the local current density and reaction overpotential, mechanical stabilization of the deposited functional material during operation, and the possibility of additional modification. Furthermore, the effortless integration of an active electrocatalyst into 3D Cu CCs makes them greatly attractive for important applications with high energy and environmental impact.

Author Contributions: Conceptualization, S.I.; formal analysis, S.I. and M.K.; writing—original draft preparation, M.K.; writing—review and editing, S.I. and M.K.; visualization, M.K.; supervision, S.I. All authors have read and agreed to the published version of the manuscript.

Funding: This research received no external funding.

Data Availability Statement: This review article does not include any new data.

Conflicts of Interest: The authors declare no conflict of interest.

Abbreviations

AAO	Anodic aluminum oxide
AC	Alternating current
ALD	Atomic layer deposition
BET	Brunauer, Emmett, and Teller theory
[BMP][TFSI]	1-Butyl-1-methylpyrrolidinium bis(trifluoromethylsulfonyl)imide
[BMP][DCA]	1-Butyl-1-methylpyrrolidinium dicyanamide
[BMIm][DCA]	1-Butyl-3-methylimidazolium dicyanamide
[BMIm][TFSI]	1-butyl-3-methylimidazolium-bis(trifluormethylsulfonyl)imide
C1	Compounds with one C atom (methane, methanol)
C2	Compounds with two C atoms (ethane, ethene, ethanol)
C3	Compounds with three C atoms (propane, propylene, propyl alcohol)
CC	Current collector
CE	Counter electrode
CTAB	Cetyltrimethylammonium bromide
Cuf	Copper foam
CV	Cyclic voltammetry
CVD	Chemical vapor deposition
3D	Three-dimensional
DC	Direct current
DETA	Diethylenetriamine
DHBT	Dynamic hydrogen bubble template
EIS	Electrochemical impedance spectroscopy

EDL	Electrical double layer
[EMIm][TFSI]	1-Ethyl-3-methylimidazolium-bis(trifluormethylsulfonyl)imide
EMIC	1-ethyl-3-methyl Imidazolium Chloride
EPD	Electrophoretic deposition
FE	Faradic efficiency
FTO	Fluorine (doped) tin oxide
HER	Hydrogen evolution reaction
IO	Inverse opal
ITO	Indium tin oxide
LIB	Li ion battery
MPSA	3-mercapto-1-propane sulfonic acid
NW	Nanowire
PC	Polycarbonate
p-Cu	Porous copper
PEG	Polyethylene glycol
PET	Polyethylene thereftalate
PVD	Physical vapor deposition
PMMA	Polymethyl methacrylate
PVDF	Polyvinylidene fluoride
PP	Polypropylene
PI	Polyimide
PS	Polystyrene
RE	Reference electrode
SCE	Saturated calomel electrode
SHE	Standard hydrogen electrode
SDS	Sodium dodecyl sulfate
SEM	Scanning electron microscopy
SS	Stainless steel
TFM	Transmission electron microscopy
TMO	Transition metal oxide
TLM	Transmission line model
UPD	Under potential deposition
WE	Working electrode
Symbols	
E^0	Equilibrium potential
A_{ECSA}	Electrochemically active surface area
C_{ref}	Area-specific reference capacitance
P	Porosity
V_{total}	Geometrical volume of material
V_{pore}	Pore volume
V_{solid}	Volume of solid metal
R_{sol}	Electrolyte bulk resistance
R_{ion}	Electrolyte resistance in the pores
C_{dl}	Electrical double layer capacitance
R_{ct}	Charge transfer resistance
ω	Angular frequency
r	Pore radius
L	Pore length
$Z_{nonfaradic}$	Non-Faradaic impedance
$Z_{faradic}$	Faradaic impedance

References

1. Zhu, P.; Gastol, D.; Marshall, J.; Sommerville, R.; Goodship, V.; Kendrick, E. A review of current collectors for lithium-ion batteries. *J. Power Source* **2021**, *485*, 229321. [CrossRef]
2. Das, M.; Biswas, A.; Purkait, T.; Boruah, T.; Bhardwaj, S.; Das, S.K.; Dey, R.S. The versatility of the dynamic hydrogen bubble template derived copper foam on the emerging energy applications: Progress and future prospects. *J. Mater. Chem. A* **2022**, *10*, 13589–13624. [CrossRef]

3. Shi, C.; Yu, M. Flexible solid-state lithium-sulfur batteries based on structural designs. *Energy Storage Mater.* **2023**, *57*, 429–459. [CrossRef]
4. Yue, Y.; Liang, H. 3D Current Collectors for Lithium-Ion Batteries: A Topical Review. *Small Methods* **2018**, *2*, 1800056. [CrossRef]
5. Kim, M.J.; Cruz, M.A.; Yang, F.; Wiley, B.J. Accelerating electrochemistry with metal nanowires. *Curr. Opin. Electrochem.* **2019**, *16*, 19–27. [CrossRef]
6. Li, D.; Chen, B.; Hu, H.; Lai, W.-Y. Constructing 3D Porous Current Collectors for Stable and Dendrite-Free Lithium Metal Anodes. *Adv. Sustain. Syst.* **2022**, *6*, 2200010. [CrossRef]
7. Shi, Q.; Lu, C.; Cao, Y.; Hao, Y.; Bachmatiuk, A.; Rümeli, M.H. Recent developments in current collectors for lithium metal anodes. *Mater. Chem. Front.* **2023**, *7*, 1298–1311. [CrossRef]
8. Wang, N.; Hang, T.; Ling, H.; Hu, A.; Li, M. High-performance Si-based 3D Cu nanostructured electrode assembly for rechargeable lithium batteries. *J. Mater. Chem. A* **2015**, *3*, 11912–11919. [CrossRef]
9. Liu, Y.; Goebla, J.; Yin, Y. Templated synthesis of nanostructured materials. *Chem. Soc. Rev.* **2013**, *42*, 2610. [CrossRef]
10. Lu, C.; Qi, L.; Yang, J.; Zhang, D.; Wu, N.; Ma, J. Simple Template-Free Solution Route for the Controlled Synthesis of $Cu(OH)_2$ and CuO Nanostructures. *J. Phys. Chem. B* **2004**, *108*, 17825–17831. [CrossRef]
11. Pu, J.; Shen, Z.; Zhong, C.; Zhou, Q.; Liu, J.; Zhu, J.; Zhang, H. Electrodeposition Technologies for Li-Based Batteries: New Frontiers of Energy Storage. *Adv. Mater.* **2020**, *32*, 1903808. [CrossRef] [PubMed]
12. Sarkar, J.; Khan, G.; Basumallick, A. Nanowires: Properties, applications, and synthesis via porous anodic aluminium oxide template. *Bull. Mater. Sci.* **2007**, *30*, 271–290. [CrossRef]
13. Masuda, H.; Fukuda, K. Ordered Metal Nanohole Arrays Made by a Two-Step Replication of Honeycomb Structures of Anodic Alumina. *Science* **1995**, *228*, 1466–1468. [CrossRef] [PubMed]
14. Lee, W.; Park, S. Porous Anodic Aluminum Oxide: Anodization and Templated Synthesis of Functional Nanostructures. *Chem. Rev.* **2014**, *114*, 7487–7556. [CrossRef]
15. Duan, H.; Gnanaraj, J.; Chena, X.; Li, B.; Lianga, J. Fabrication and characterization of Fe_3O_4-based Cu nanostructured electrode for Li-ion battery. *J. Power Source* **2008**, *185*, 512–518. [CrossRef]
16. Davydov, N.D.; Sattari, P.A.; AlMawlawi, D.; Osika, A.; Haslett, T.L.; Moskovits, M. Field emitters based on porous aluminum oxide templates. *J. Appl. Phys.* **1999**, *86*, 3983–3987. [CrossRef]
17. Li, X.; Wang, Y.; Song, G.; Peng, Z.; Yu, Y.; She, X.; Sun, J.; Li, J.; Li, P.; Wang, Z.; et al. Fabrication and Magnetic Properties of Ni/Cu Shell/Core Nanocable Arrays. *J. Phys. Chem. C* **2010**, *114*, 6914–6916. [CrossRef]
18. Chang, R.; Zheng, L.; Wang, C.; Yang, D.; Zhang, G.; Sun, S. Synthesis of Hierarchical Platinum-Palladium-Copper Nanodendrites for Efficient Methanol Oxidation. *Appl. Catal. B* **2017**, *211*, 205–211. [CrossRef]
19. Sulka, G.D.; Stroobants, S.; Moshchalkov, V.; Borghs, G.; Celisd, J. Synthesis of Well-Ordered Nanopores by Anodizing Aluminum Foils in Sulfuric Acid. *J. Electrochem. Soc.* **2002**, *149*, D97–D103. [CrossRef]
20. Sulka, G.D.; Stepniowski, W. Structural features of self-organized nanopore arrays formed by anodization of aluminum in oxalic acid at relatively high temperatures. *Electrochim. Acta* **2009**, *54*, 3683–3691. [CrossRef]
21. Zaraska, L.; Sulka, G.D.; Jaskuła, M. The effect of n-alcohols on porous anodic alumina formed by self-organized two-step anodizing of aluminum in phosphoric acid. *Surf. Coat. Technol.* **2010**, *204*, 1729–1737. [CrossRef]
22. Zaraska, L.; Sulka, G.D.; Jaskuła, M. Fabrication of free-standing copper foils covered with highly-ordered copper nanowire arrays. *Appl. Surf. Sci.* **2012**, *258*, 7781–7786. [CrossRef]
23. Eftekhari, A. (Ed.) *Nanostructured Materials in Electrochemistry*; Wiley-VCH: Weinheim, Germany, 2008; pp. 1–116, ISBN 978-3-527-31876-6.
24. Chowdhury, T.; Casey, D.P.; Rohan, J.F. Additive influence on Cu nanotube electrodeposition in anodised aluminium oxide templates. *Electrochem. Commun.* **2009**, *11*, 1203–1206. [CrossRef]
25. Gerein, N.J.; Haber, J.A. Effect of ac Electrodeposition Conditions on the Growth of High Aspect Ratio Copper Nanowires in Porous Aluminum Oxide Templates. *J. Phys. Chem. B* **2005**, *109*, 17372–17385. [CrossRef] [PubMed]
26. Gelves, G.A.; Lin, B.; Sundararaj, U.; Haber, J.A. Low Electrical Percolation Threshold of Silver and Copper Nanowires in Polystyrene Composites. *Adv. Funct. Mater.* **2006**, *16*, 2423–2430. [CrossRef]
27. Taberna, P.L.; Mitra, S.; Poizot, P.; Simon, P.; Tarascon, J.-M. High rate capabilities Fe_3O_4-based Cu nano-architectured electrodes for lithium-ion battery applications. *Nat. Mater.* **2006**, *5*, 567–573. [CrossRef]
28. Ramírez, C.; Bozzini, B.; Calderón, J.A. Electrodeposition of copper from triethanolamine as a complexing agent in alkaline solution. *Electrochim. Acta* **2022**, *425*, 140654. [CrossRef]
29. Chen, X.; Duan, H.; Zhou, Z.; Liang, J.; Gnanaraj, J. Fabrication of free-standing Cu nanorod arrays on Cu disc by template-assisted electrodeposition. *Nanotechnology* **2008**, *19*, 365306. [CrossRef]
30. Liu, H.; Meng, Y.S.; Li, Q. Three-dimensional nanocable arrays with a copper core and cupric oxide shell for high power lithium ion batteries. *RSC Adv.* **2013**, *3*, 11586–11593. [CrossRef]
31. Rehnlund, D.; Pettersson, J.; Edström, K.; Nyholm, L. Lithium Trapping in Microbatteries Based on Lithium- and Cu_2O-Coated Copper Nanorods. *ChemistrySelect* **2018**, *3*, 2311–2314. [CrossRef]
32. Brzózka, A.; Szeliga, D.; Kurowska-Tabor, E.; Sulka, G.D. Synthesis of copper nanocone array electrodes and its electrocatalytic properties toward hydrogen peroxide reduction. *Mater. Lett.* **2016**, *174*, 66–70. [CrossRef]

33. Huang, B.-R.; Yeh, C.-S.; Wang, D.-C.; Tan, J.T.; Sung, J. Field emission studies of amorphous carbon deposited on copper nanowires grown by cathodic arc plasma deposition. *New Carbon Mater.* **2009**, *24*, 97–101. [CrossRef]
34. Lim, J.; Kim, K.-H.; Cojocaru, C.-S. Highly uniform, straightforward, controllable fabrication of copper nano-objects via artificial nucleation-assisted electrodeposition. *J. Electroanal. Chem.* **2021**, *897*, 1155946. [CrossRef]
35. Teshima, H.; Kojima, K.; Ju, Y. Fabrication of Anodic Aluminum Oxide Template and Copper Nanowire Surface Fastener. *J. Electron. Packag.* **2014**, *136*, 044501. [CrossRef]
36. Stepniowski, W.J.; Moneta, M.; Karczewski, K.; Michalska-Domanska, M.; Czujko, T.; Mol, J.M.C.; Buijnsters, J.G. Fabrication of copper nanowires via electrodeposition in anodic aluminum oxide templates formed by combined hard anodizing and electrochemical barrier layer thinning. *J. Electroanal. Chem.* **2018**, *809*, 59–66. [CrossRef]
37. Ma, T.; Janot, J.-M.; Balme, S. Track-Etched Nanopore/Membrane: From Fundamental to Applications. *Small Methods* **2020**, *4*, 2000366. [CrossRef]
38. Fleischer, R.L.; Price, P.B.; Symes, E.M. Novel Filter for Biological Materials. *Science* **1964**, *143*, 249–250. [CrossRef]
39. Motoyama, M.; Fukunaka, Y.; Sakka, T.; Ogata, Y.H.; Kikuchi, S. Electrochemical processing of Cu and Ni nanowire arrays. *J. Electroanal. Chem.* **2005**, *584*, 84–91. [CrossRef]
40. Chlebny, I.; Doudin, B.; Ansermet, J.-P. Pore size distributions of nanoporous track-etched membranes. *Nanostructured Mater.* **1993**, *2*, 637–642. [CrossRef]
41. Azarian, A.; Irajizad, A.; Dolati, A.; Ghorbani, M. Time dependence of the surface plasmon resonance of copper nanorods. *J. Phys. Condens. Matter* **2007**, *19*, 446007. [CrossRef]
42. Enculescu, I.; Siwy, Z.; Dobrev, D.; Trautmann, C.; Toimil Molares, M.-E.; Neumann, R.; Hjort, K.; Westerberg, L.; Spohr, R. Copper nanowires electrodeposited in etched single-ion track templates. *Appl. Phys. A* **2003**, *77*, 751–755. [CrossRef]
43. Kaur, R.; Verma, N.K.; Kumar, S. Fabrication of copper microcylinders in polycarbonate membranes and their characterization. *J. Mater. Sci.* **2006**, *41*, 3723–3728. [CrossRef]
44. Kaur, R.; Singh, S.; Kaur, J.; Kumar, R. Study of Variation in Pore Diameter with Etching Rate and Fabrication of Copper Nano/Micro Wires Using Electrodeposition Method. *Polym. Plast. Technol. Eng.* **2012**, *51*, 1193–1197. [CrossRef]
45. Motoyama, M.; Fukunaka, Y.; Sakka, T.; Ogata, Y.H. Initial stages of electrodeposition of metal nanowires in nanoporous templates. *Electrochim. Acta* **2007**, *53*, 205–212. [CrossRef]
46. Riveros, G.; Gómez, H.; Schrebler, R.; Marotti, R.E.; Dalchiele, E.A. An In Situ EIS Study during the Electrochemical Growth of Copper Nanowires into Porous Polycarbonate Membranes. *Electrochem. Solid-State Lett.* **2008**, *11*, K19–K23. [CrossRef]
47. Dauginet-De Pra, L.; Ferain, E.; Legras, R.; Demoustier-Champagne, S. Fabrication of a new generation of track-etched templates and their use for the synthesis of metallic and organic nanostructures. *Nucl. Instrum. Methods Phys. Res. Sect. B* **2002**, *196*, 81–88. [CrossRef]
48. Duan, J.; Liu, J.; Mo, D.; Yao, H.; Maaz, K.; Chen, Y.; Sun, Y.; Hou, M.; Qu, X.; Zhang, L.; et al. Controlled crystallinity and crystallographic orientation of Cu nanowires fabricated in ion-track templates. *Nanotechnology* **2010**, *21*, 365605. [CrossRef]
49. Gambirasia, A.; Cattarin, S.; Musiani, M.; Vázquez-Gómeza, L.; Verlatoa, L. Direct electrodeposition of metal nanowires on electrode surface. *Electrochim. Acta* **2011**, *56*, 8582–8588. [CrossRef]
50. Denkov, N.D.; Velev, O.D.; Kralchevsky, P.A.; Ivanov, I.B.; Yoshimura, H.; Nagayama, K. Mechanism of Formation of Two-Dimensional Crystals from Latex Particles on Substrates. *Langmuir* **1992**, *8*, 3183–3190. [CrossRef]
51. Juárez, B.H.; García, P.D.; Golmayo, D.; Blanco, A.; López, C. ZnO Inverse Opals by Chemical Vapor Deposition. *Adv. Mater.* **2005**, *17*, 2761–2765. [CrossRef]
52. Wijnhoven, J.E.G.J.; Zevenhuizen, S.J.M.; Hendriks, M.A.; Vanmaekelbergh, D.; Kelly, J.J.; Vos, W.L. Electrochemical Assembly of Ordered Macropores in Gold. *Adv. Mater.* **2000**, *12*, 888. [CrossRef]
53. Ding, L.; Yu-Ren, W.; Yong, Y.; Wen-Jie, M.; Cheng, L. Improving nucleation in the fabrication of high-quality 3D macro-porous copper film through the surface-modification of a polystyrene colloid-assembled template. *Chin. Phys.* **2007**, *16*, 468. [CrossRef]
54. Ding, L.; Yuren, W.; Wenjie, M.; He, C.; Taohua, X.; Can, Y. The key factors in fabrication of high-quality ordered macroporous copper film. *Appl. Surf. Sci.* **2008**, *254*, 6775–6778. [CrossRef]
55. Barako, M.T.; Weisse, J.M.; Roy, S.; Kodama, T.; Dusseault, T.J.; Motoyama, M.; Asheghi, M.; Prinz, F.B.; Zheng, X.; Goodson, K.E. Thermal conduction in nanoporous copper inverse opal films. In Proceedings of the Fourteenth Intersociety Conference on Thermal and Thermomechanical Phenomena in Electronic Systems (ITherm), Orlando, FL, USA, 27–30 May 2014; pp. 736–743. [CrossRef]
56. Tsai, M.-C.; Zhuanga, D.-X.; Chen, P.-Y. Electrodeposition of macroporous silver films from ionic liquids and assessment of these films in the electrocatalytic reduction of nitrate. *Electrochim. Acta* **2010**, *55*, 1019–1027. [CrossRef]
57. El Abedin, S.Z.; Prowald, A.; Endres, F. Fabrication of highly ordered macroporous copper films using template-assisted electrodeposition in an ionic liquid. *Electrochem. Commun.* **2012**, *18*, 70–72. [CrossRef]
58. Bassetto, V.C.; Russell, A.E.; Kubota, L.T.; Bartlett, P.N. Preparation of copper sphere segment void templates for electrochemical SERS and their use to study the interaction of amino acids with copper under potentiostatic control. *Electrochim. Acta* **2014**, *144*, 400–405. [CrossRef]
59. Song, H.; Im, M.; Song, J.T.; Lim, J.-A.; Kim, B.S.; Kwo, Y.; Jihun, S.R. Effect of Mass Transfer and Kinetics in Ordered Cu-Mesostructures for Electrochemical CO_2 Reduction. *Appl. Catal. B Environ.* **2018**, *232*, 391–396. [CrossRef]

60. Zhang, C.; Palko, J.W.; Rong, G.; Pringle, K.S.; Barako, M.T.; Dusseault, T.J.; Asheghi, M.; Santiago, J.G.; Goodson, K.E. Tailoring Permeability of Microporous Copper Structures through Template Sintering. *ACS Appl. Mater. Interfaces* **2018**, *10*, 30487–30494. [CrossRef]
61. Wu, H.; Zheng, L.; Liu, W.; Xia, X.; Xiao, C.; Xie, J.; Su, L.; Wang, L.; Du, N. Three-dimensional porous copper framework supported group IVA element materials as sodium-ion battery anode materials. *J. Alloys Compd.* **2019**, *771*, 169–175. [CrossRef]
62. Meng, X.; Song, Y.; Shu, T. Morphology control and optical characterization of three-dimensional ordered macroporous Cu films from template-assisted electrodeposition. *J. Porous Mater.* **2020**, *27*, 1069–1076. [CrossRef]
63. Zhou, Y.; Zhao, J.; Liu, Y.; Ng, R.J.H.; Yang, J.K.W. Optical and electrochemical properties of 3D nanoporous Cu_2O-Cu inverse opal structures tuned by electrodeposition. *Mater. Sci. Semicond. Process.* **2021**, *121*, 105444. [CrossRef]
64. Niu, J.; Liu, X.; Xia, K.; Xu, L.; Xu, Y.; Fang, X.; Lu, W. Effect of Electrodeposition Parameters on the Morphology of Three-Dimensional Porous Copper Foams. *Int. J. Electrochem. Sci.* **2015**, *10*, 7331–7340.
65. Atchison, S.N.; Burford, R.P.; Whitby, C.P.; Hibbert, D.B. Electrodeposition of copper in quasi-two dimensions from solutions containing sodium sulfate. *J. Electroanal. Chem.* **1995**, *399*, 71–77. [CrossRef]
66. Lopez-Salvans, M.-Q.; Sagues, F.; Claret, J.; Bassas, J. Fingering instability in thin-layer electrodeposition: General trends and morphological transitions. *J. Electroanal. Chem.* **1997**, *421*, 205–212. [CrossRef]
67. Shin, H.-C.; Liu, M. Copper Foam Structures with Highly Porous Nanostructured Walls. *Chem. Mater.* **2004**, *16*, 5460–5464. [CrossRef]
68. Li, Y.; Jia, W.-Z.; Song, Y.-Y.; Xia, X.-H. Superhydrophobicity of 3D Porous Copper Films Prepared Using the Hydrogen Bubble Dynamic Template. *Chem. Mater.* **2007**, *19*, 5758–5764. [CrossRef]
69. Kim, J.-H.; Kim, R.-H.; Kwon, H.-S. Preparation of copper foam with 3-dimensionally interconnected spherical pore network by electrodeposition. *Electrochem. Commun.* **2008**, *10*, 1148–1151. [CrossRef]
70. Kurniawan, M.; Stich, M.; Marimon, M.; Camargo, M.; Peipmann, R.; Hannappel, T.; Bund, A. Electrodeposition of cuprous oxide on a porous copper framework for an improved photoelectrochemical performance. *J. Mater. Sci.* **2021**, *56*, 11866–11880. [CrossRef]
71. Shin, H.-C.; Dong, J.; Liu, M. Nanoporous structures prepared by an electrochemical deposition process. *Adv. Mater.* **2003**, *15*, 1610–1614. [CrossRef]
72. Umh, H.N.; Park, J.; Yeob, J.; Jung, S.; Nam, I.; Yi, J. Lithium metal anode on a copper dendritic superstructure. *Electrochem. Commun.* **2019**, *99*, 27–31. [CrossRef]
73. Yang, H.; Hao, X.; Tang, X.; Jin, W.; Liu, C.; Hou, H.; Ji, H.; Hu, J. Dual-functional porous copper films modulated via dynamic hydrogen bubble template for in situ SERS monitoring electrocatalytic reaction. *Appl. Surf. Sci.* **2019**, *494*, 731–739. [CrossRef]
74. Keir, D.S.; Pryor, M.J. The Dealloying of Copper-Manganese Alloys. *J. Electrochem. Soc. Electrochem. Sci. Technol.* **1980**, *127*, 2138–2144. [CrossRef]
75. Zhang, Q.B.; Abbott, A.; Yang, C. Electrochemical fabrication of nanoporous copper films in choline chloride-urea deep eutectic solvent. *Phys. Chem. Chem. Phys.* **2015**, *17*, 14702–14709. [CrossRef] [PubMed]
76. Pryor, M.J.; Fister, J.C. The Mechanism of Dealloying of Copper Solid Solutions and Intermetallic Phases. *J. Electrochem. Soc. Electrochem. Sci. Technol.* **1984**, *131*, 1230–1235. [CrossRef]
77. Lin, Y.-W.; Tai, C.-C.; Sun, I.-W. Electrochemical Preparation of Porous Copper Surfaces in Zinc Chloride-1-ethyl-3-methyl Imidazolium Chloride Ionic Liquid. *J. Electrochem. Soc.* **2007**, *154*, D316–D321. [CrossRef]
78. Al-Kharafi, F.M.; Ateya, B.G.; Abd Allah, R.M. Selective dissolution of brass in salt water. *J. Appl. Electrochem.* **2004**, *34*, 47–53. [CrossRef]
79. Luan, C.; Chen, L.; Li, B.; Zhu, L.; Li, W. Electrochemical Dealloying-Enabled 3D Hierarchical Porous Cu Current Collector of Lithium Metal Anodes for Dendrite Growth Inhibition. *ACS Appl. Energy Mater.* **2021**, *4*, 13903–13911. [CrossRef]
80. Zhang, Q.; Zhang, Z. On the electrochemical dealloying of Al-based alloys in a NaCl aqueous solution. *Phys. Chem. Chem. Phys.* **2010**, *12*, 1453–1472. [CrossRef]
81. Song, T.; Yan, M.; Shi, Z.; Atrens, A.; Qian, M. Creation of bimodal porous copper materials by an annealing-electrochemical dealloying approach. *Electrochim. Acta* **2015**, *164*, 288–296. [CrossRef]
82. Lu, H.-B.; Li, Y.; Wang, F.-H. Synthesis of porous copper from nanocrystalline two-phase Cu-Zr film by dealloying. *Scr. Mater.* **2007**, *56*, 165–168. [CrossRef]
83. Spassov, T.; Lyubenova, L.; Liu, Y.; Bliznakov, S.; Spassova, M.; Dimitrov, N. Mechanochemical synthesis, thermal stability and selective electrochemical dissolution of Cu-Ag solid solutions. *J. Alloys Compd.* **2009**, *478*, 232–236. [CrossRef]
84. Luo, X.; Li, R.; Huang, L.; Zhang, T. Nucleation and growth of nanoporous copper ligaments during electrochemical dealloying of Mg-based metallic glasses. *Corros. Sci.* **2013**, *67*, 100–108. [CrossRef]
85. Chang, X.; Liu, H.; Yang, H.; Di, J.; Tang, W.; Fu, H.; Li, M.; Liu, R. Co-guiding the dendrite-free plating of lithium on lithiophilic ZnO and fluoride modified 3D porous copper for stable Li metal anode. *J. Mater.* **2020**, *6*, 54–61. [CrossRef]
86. Reyter, D.; Odziemkowski, M.; Belanger, D.; Roue, L. Electrochemically Activated Copper Electrodes Surface Characterization, Electrochemical Behavior, and Properties for the Electroreduction of Nitrate. *J. Electrochem. Soc.* **2007**, *154*, K36–K44. [CrossRef]
87. Reyter, D.; Rousselot, S.; Mazouzi, D.; Gauthier, M.; Moreau, P.; Lestriez, B.; Guyomard, D.; Roue, L. An electrochemically roughened Cu current collector for Si-based electrode in Li-ion batteries. *J. Power Source* **2013**, *239*, 308–314. [CrossRef]

88. Wang, T.-S.; Liu, Y.; Lu, Y.-X.; Hu, Y.-S.; Fan, L.-Z. Dendrite-free Na metal plating/stripping onto 3D porous Cu hosts. *Energy Storage Mater.* **2018**, *15*, 274–281. [CrossRef]
89. Chen, J.; Yang, L.; Fang, S.; Hirano, S.; Tachibana, K. Three-dimensional core-shell Cu@Cu6Sn5 nanowires as the anode material for lithium ion batteries. *J. Power Source* **2012**, *199*, 341–345. [CrossRef]
90. Pauric, A.D.; Baig, S.A.; Pantaleo, A.N.; Wang, Y.; Kruse, P. Sponge-Like Porous Metal Surfaces from Anodization in Very Concentrated Acids. *J. Electrochem. Soc.* **2013**, *160*, C12–C18. [CrossRef]
91. Pham, Q.N.; Shao, B.; Kim, Y.; Won, Y. Hierarchical and Well-Ordered Porous Copper for Liquid Transport Properties Control. *ACS Appl. Mater. Interfaces* **2018**, *10*, 16015–16023. [CrossRef]
92. Celante, V.G.; Freitas, M.B.J.G. Electrodeposition of copper from spent Li-ion batteries by electrochemical quartz crystal microbalance and impedance spectroscopy techniques. *J. Appl. Electrochem.* **2010**, *40*, 233–239. [CrossRef]
93. Peng, C.; Yang, L.; Fang, S.; Wang, J.; Zhang, Z.; Tachibana, K.; Yang, Y.; Zhao, S. Electrochemical behavior of copper current collector in imidazolium-based ionic liquid electrolytes. *J. Appl. Electrochem.* **2010**, *40*, 653–662. [CrossRef]
94. Giri, S.D.; Sarkar, A. Estimating surface area of copper powder: A comparison between electrochemical, microscopy and laser diffraction methods. *Adv. Power Technol.* **2018**, *29*, 3520–3526. [CrossRef]
95. Zhang, J.; Sung, Y.-E.; Rikvold, P.A.; Wieckowski, A. Underpotential deposition of Cu on Au(111) in sulfate-containing electrolytes: A theoretical and experimental study. *J. Chem. Phys.* **1996**, *104*, 5699–5712. [CrossRef]
96. Aldana-González, J.; Olvera-García, J.; Montes de Oca, M.G.; Romero-Romo, M.; Ramírez-Silva, M.T.; Palomar-Pardavé, M. Electrochemical quantification of the electro-active surface area of Au nanoparticles supported onto an ITO electrode by means of Cu UPD. *Electrochem. Commun.* **2015**, *56*, 70–74. [CrossRef]
97. Łukaszewski, M.; Soszko, M.; Czerwinski, A. Electrochemical methods of real surface area determination of noble metal electrodes—An overview. *Int. J. Electrochem. Sci.* **2016**, *11*, 4442–4469. [CrossRef]
98. Giri, S.D.; Sarkar, A. Electrochemical study of bulk and monolayer copper in alkaline solution. *J. Electrochem. Soc.* **2016**, *163*, H252–H259. [CrossRef]
99. Fletcher, S.; Barradas, R.G.; Porter, J.D. The anodic oxidation of copper amalgam and polycrystalline copper electrodes in LiOH solution. *J. Electrochem. Soc.* **1978**, *125*, 1960. [CrossRef]
100. Zankowski, S.; Vereecken, P.M. Electrochemical Determination of Porosity and Surface Area of Thin Films of Interconnected Nickel Nanowires. *J. Electrochem. Soc.* **2019**, *166*, D227–D235. [CrossRef]
101. Ogihara, N.; Itou, Y.; Sasaki, T.; Takeuchi, Y. Impedance Spectroscopy Characterization of Porous Electrodes under Different Electrode Thickness Using a Symmetric Cell for High-Performance Lithium-Ion Batteries. *J. Phys. Chem. C* **2015**, *119*, 4612–4619. [CrossRef]
102. de Levie, R. On Porous Electrodes in Electrolyte Solutions. *Electrochim. Acta* **1963**, *8*, 751–780. [CrossRef]
103. de Levie, R. On Porous Electrodes in Electrolyte Solutions Iv. *Electrochim. Acta* **1964**, *9*, 1231–1245. [CrossRef]
104. Lasia, A. *Electrochemical Impedance Spectroscopy and Its Applications*; Springer: New York, NY, USA, 2014. [CrossRef]
105. Hansen, J.N.; Prats, H.; Toudahl, K.K.; Secher, N.M.; Chan, K.; Kibsgaard, J.; Chorkendorff, I. Is There Anything Better Than Pt for HER? *ACS Energy Lett.* **2021**, *6*, 1175–1180. [CrossRef]
106. Rezaei, B.; Mokhtarianpour, M.; Ensafi, A.A. Fabricated of bimetallic Pd/Pt nanostructure deposited on copper nanofoam substrate by galvanic replacement as an effective electrocatalyst for hydrogen evolution reaction. *Int. J. Hydrogen Energy* **2015**, *49*, 6754–6762. [CrossRef]
107. Das, M.; Jena, N.; Purkait, T.; Kamboj, N.; Sarkar, A.D.; Dey, R.S. Single-phase Ni_5P_4-copper foam superhydrophilic and aerophobic core-shell nanostructures for efficient hydrogen evolution reaction. *J. Mater. Chem. A* **2019**, *7*, 23989–23999. [CrossRef]
108. Vesztergom, S.; Dutta, A.; Rahaman, M.; Kiran, K.; Montiel, I.Z.; Broekmann, P. Hydrogen Bubble Templated Metal Foams as Efficient Catalysts of CO_2 Electroreduction. *ChemCatChem* **2021**, *13*, 1039–1058. [CrossRef]
109. Todorova, T.K.; Schreiber, M.W.; Fontecave, M. Mechanistic Understanding of CO_2 Reduction Reaction (CO_2RR) toward Multicarbon Products by Heterogeneous Copper-Based Catalysts. *ACS Catal.* **2020**, *10*, 1754–1768. [CrossRef]
110. Lin, D.; Liu, Y.; Cui, Y. Reviving the lithium metal anode for high-energy batteries. *Nat. Nanotechnol.* **2017**, *12*, 194–206. [CrossRef]
111. Niu, C.; Liu, D.; Lochala, J.A.; Anderson, C.S.; Cao, X.; Gross, M.E.; Xu, W.; Zhang, J.-G.; Whittingham, M.S.; Xiao, J.; et al. Balancing interfacial reactions to achieve long cycle life in high-energy lithium metal batteries. *Nat. Energy* **2021**, *6*, 723–732. [CrossRef]
112. Ning, Z.; Li, G.; Melvin, D.L.R.; Chen, Y.; Bu, J.; Spencer-Jolly, D.; Liu, J.; Hu, B.; Gao, X.; Perera, J.; et al. Dendrite initiation and propagation in Li-metal solid-state batteries. *Nature* **2023**, *618*, 287–293. [CrossRef]
113. Qiu, H.; Tang, T.; Asif, M.; Huang, X.; Hou, Y. 3D Porous Cu Current Collectors Derived by Hydrogen Bubble Dynamic Template for Enhanced Li Metal Anode Performance. *Adv. Funct. Mater.* **2019**, *29*, 1808468. [CrossRef]
114. Chen, L.; Wang, M.; Lv, A.; Hu, W.; Jiao, S. Self-Supporting Dendritic Copper Porous Film Inducing the Lateral Growth of Metallic Lithium for Highly Stable Li Metal Battery. *J. Electrochem. Soc.* **2019**, *166*, A4073–A4079. [CrossRef]
115. Kim, Y.; Jeong, S.; Bae, H.E.; Tron, A.; Sung, Y.-E.; Mun, J.; Kwon, O.J. Electrochemical behavior of residual salts and an effective method to remove impurities in the formation of porous copper electrode for lithium metal batteries. *Int. J. Energy Res.* **2021**, *45*, 10738–10745. [CrossRef]
116. Choi, B.N.; Seo, J.Y.; Kim, B.; Kim, Y.S.; Chun, C.-H. Electro-deposition of the lithium metal anode on dendritic copper current collectors for lithium battery application. *Appl. Surf. Sci.* **2020**, *506*, 144884. [CrossRef]

117. Chen, J.; Qiao, X.; Fu, W.; Han, X.; Wu, Q.; Wang, Y.; Zhang, Y.; Shi, L.; Zhao, J.; Ma, Y. Lithiophilic hyperbranched Cu nanostructure for stable Li metal anodes. *SmartMat.* **2023**, *4*, e1174. [CrossRef]
118. Zhang, D.; Dai, A.; Fan, B.; Li, Y.; Shen, K.; Xiao, T.; Hou, G.; Cao, H.; Tao, X.Y.; Tang, Y. Three-Dimensional Ordered Macro/Mesoporous Cu/Zn as a Lithiophilic Current Collector for Dendrite-Free Lithium Metal Anode. *ACS Appl. Mater. Interfaces* **2020**, *12*, 31542–31551. [CrossRef]
119. Zhao, H.; Lei, D.; He, Y.-B.; Yuan, Y.; Yun, Q.; Ni, B.; Lv, W.; Li, B.; Yang, Q.-H.; Kang, F.; et al. Compact 3D Copper with Uniform Porous Structure Derived by Electrochemical Dealloying as Dendrite-Free Lithium Metal Anode Current Collector. *Adv. Energy Mater.* **2018**, *8*, 1800266. [CrossRef]
120. Tang, Y.; Shen, K.; Lv, Z.; Xu, X.; Hou, G.; Cao, H.; Wu, L.; Zheng, L.; Deng, Y. Three-dimensional ordered macroporous Cu current collector for lithium metal anode: Uniform nucleation by seed crystal. *J. Power Source* **2018**, *403*, 82–89. [CrossRef]
121. Qi, M.; Xie, L.; Han, Q.; Zhu, L.; Chen, L.; Cao, C. An overview of the key challenges and strategies for lithium metal anodes. *J. Energy Storage* **2022**, *47*, 103641. [CrossRef]
122. Suk, J.; Kim, D.Y.; Kim, D.W.; Kang, Y. Electrodeposited 3D porous silicon/copper films with excellent stability and high rate performance for lithium-ion batteries. *J. Mater. Chem. A* **2014**, *2*, 2478. [CrossRef]
123. Dogan, F.; Sanjeewa, L.D.; Hwub, S.-J.; Vaughey, J.T. Electrodeposited Copper Foams as Substrates for Thin Film Silicon Electrodes. *Solid State Ion.* **2016**, *288*, 204–206. [CrossRef]
124. Link, S.; Kurniawan, M.; Dimitrova, A.; Krischok, S.; Bund, A.; Ivanov, S. Enhanced cycling performance of binder free silicon-based anode by application of electrochemically formed microporous substrate. *Electrochim. Acta* **2021**, *380*, 138216. [CrossRef]
125. Mirzaee, M.; Dehghanian, C. Synthesis of nanoporous copper foam-applied current collector electrode for supercapacitor. *J. Iran. Chem. Soc.* **2019**, *16*, 283–292. [CrossRef]
126. Eugenio, S.; Silva, T.; Carmezim, M.; Duarte, R.; Montemor, M. Electrodeposition and characterization of nickel-copper metallic foams for application as electrodes for supercapacitors. *J. Appl. Electrochem.* **2014**, *44*, 455–465. [CrossRef]
127. Lange, G.; Eugenio, S.; Duarte, R.; Silva, T.; Carmezim, M.; Montemor, M.d.F. Characterisation and electrochemical behaviour of electrodeposited Cu–Fe foams applied as pseudocapacitor electrodes. *J. Electroanal. Chem.* **2015**, *737*, 85–92. [CrossRef]